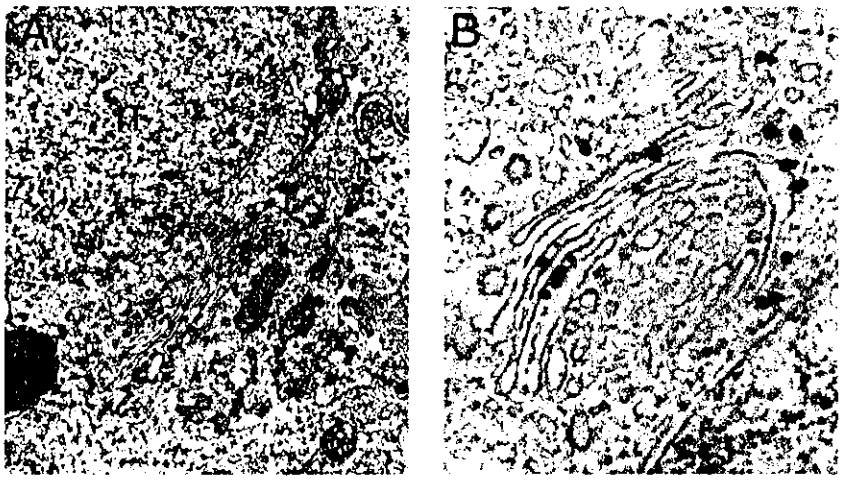

Figure 7. HIP14 immunogold labeling of medial Golgi. (**A**) A micrograph of HIP14 immunogold labeling in a mouse cortical neuron. Immunogold particles are mostly associated with the cisternae stacks of the Golgi apparatus. A few particles are associated with coated vesicles in the surrounding cytoplasm. No particles were seen in the nucleus. (**B**) High magnification of a Golgi apparatus with many immunogold particles associated with the medial Golgi cisternae and some staining associated with the *cis* and *trans* cisternae. Scale: (A) 1 μm; (B) 160 nm.

shown to play a role in the internalization of several mammalian proteins as well (26,27). Ubiquitination, and the subsequent internalization and degradation, are thought to be the critical mechanism in the down-regulation of several receptors at the plasma membranes of mammalian cells (28). Since HIP14 can functionally compensate for the loss of activity of Akr1p, it is likely to have a similar role as Akr1p in the sorting or targeting of critical proteins involved in the initiating events of endocytosis at the plasma membrane.

Interestingly, HIP14 is not the only protein with which htt interacts that has been implicated in intracellular transport. Other htt-interacting proteins with roles in intracellular transport include α-adaptin, a component of the AP-2 complex that binds to clathrin and is involved in endocytosis at the plasma membrane (25), and HAP1 (9), which in turn binds to the $p150^{Glued}$ subunit of dynactin (29), a protein involved in retrograde transport. HAP1 is also directly involved in the regulation of vesicular trafficking from early endosomes to the late endocytic compartment (11). htt has also been shown to bind HIP1 (21), whose yeast homologue (Sla2p) mutants show defects in endocytosis and cytoskeletal organization (30,31). HIP1 has been recently shown to bind to F-actin, clathrin and adaptor protein 2 (32–35), all of which are proteins essential for vesicle assembly and cytoskeletal organization in mammalian cells, thus providing further evidence for similar functions between mammalian and yeast homologues in intracellular transport pathways. In addition, htt interacts with SH3GL3, a protein belonging to the SH3 domain-containing protein family that plays a role in synaptic vesicle transport (13). Interestingly, HAP1, HIP1, SH3GL3 and HIP14 all show altered interactions with mutant htt, supporting the possibility that the pathogenesis in HD involves dysfunction in intracellular transport in the affected neurons. Our study provides additional evidence for the role of htt in intraneuronal transport processes.

Several putative functions have been suggested for htt. These include roles in transcriptional regulation, intracellular transport and cell cycle regulation. Interestingly, almost all of htt's interaction partners implicated in the functions of intracellular transport and transcriptional regulation show altered interaction with htt in the presence of the poly(Q) expansion, thus implicating disturbance of these two proposed functions of htt as contributing to the pathogenesis in HD. In contrast, htt does not show altered interactions with proteins such as HIP2 and p53, suggesting that the functions of htt in cell cycle control and cell survival is part of its normal function, and do not contribute directly to the pathogenesis. The isolation and characterization of HIP14 as an htt-interacting protein with altered interaction in the presence of the mutation, together with the fact that htt and HIP14 co-localize, and that HIP14 is able to rescue the defect in endocytosis in *Akr1Δ* cells, suggests another link in the function of htt in intracellular transport and endocytosis. Although important, this study does not provide a clear mechanism as to how an HIP14-expanded htt interaction could contribute to the selective vulnerability of cortical and striatal neurons in HD. However, altered interactions with HIP14 caused by the mutation in htt further implicate altered pathways of intraneuronal transport and endocytosis in the pathology of HD, a hypothesis that now deserves formal assessment.

MATERIALS AND METHODS

Yeast two-hybrid screening

The N-terminal htt plasmid construct pGBT9–1955-44 (16) was transformed into the yeast strain Y190 (*MATa, ura3-52, his3-200, ade2-101, lys2-801, trp1-901, leu2-3, 112, gal4Δ, gal80Δ, cyh^{r}2, LYS2::GAL1$_{UAS}$- HIS3$_{TATA}$-HIS3, URA3::GAL1$_{UAS}$-GAL1$_{TATA}$-lacZ*). A human adult brain Matchmaker cDNA library (Clontech) was then transformed into Y190 cells already harboring the pGBT9–1955-44 construct (36). The transformants were plated onto synthetic complete (SC) medium (Trp^-/Leu^-/His^-) with 25 mM of

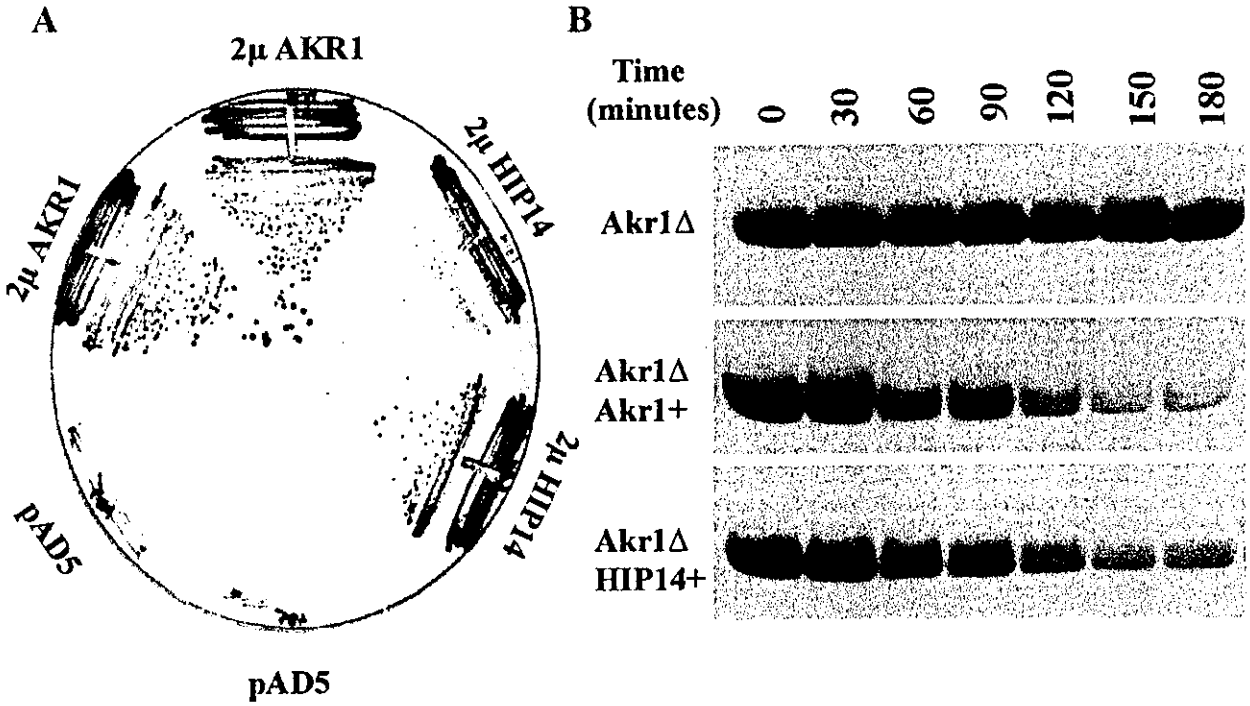

Figure 8. HIP14 functions in endocytosis in yeast. *HIP14* (pAD5–HIP14), AKR1 (pPB575) and a control vector (pAD5) were transformed into *akr1Δ* cells that show a temperature sensitive phenotype when AKR1 is deleted. (A) In the presence of either Akr1p (positive control) or HIP14, there is a rescue of the temperature-sensitive phenotype displayed by *akr1Δ* cells, as seen by the restored growth of yeast colonies. (B) HIP14 rescues the Ste3p endocytosis defect in *akr1Δ* cells, as indicated by the more rapid disappearance of the Ste3p band in cells carrying pAD5–HIP14 as compared with pAD5. The *akr1Δ* cells containing either control vector (pAD5), HIP14 or AKR1 were incubated with cycloheximide to prevent the synthesis of proteins. The expression of the yeast protein Ste3p was detected by immunoblotting. In cells with control vector, there is no endocytosis of Ste3p and consequently no disappearance of the Ste3 protein over time. In the positive control AKR1 containing cells, endocytosis occurs as shown by the disappearance of the Ste3 protein. In HIP14 cells, endocytosis also occurs, proving that HIP14 is able to rescue a defect in endocytosis in yeast.

3-aminotriazole (3-AT) to suppress the growth of false His^+ colonies. β-Galactosidase filter assays were performed, and the plasmids containing activating domain cDNAs were isolated by electroporating the bacterial strain KC8 with the yeast lysate (37). The resulting colonies were transformed into DH5-α for further manipulation.

Yeast two-hybrid interactions

The yeast strain Y190 was co-transformed with pGAD*HIP14*-500, the clone isolated from the yeast two hybrid library screen, and pGBT9–1955-15, pGBT9–1955-128 (38) or pGBT9 using a modified lithium acetate transformation protocol as described previously (36). β-Galactosidase chromogenic filter assays (16,37) and semiquantitative liquid assays using *o*-nitrophenyl-β-D-galactopyranoside (ONPG) as a substrate were performed as recommended (Clontech). Statistical analyses were performed using the Newman–Keuls multiple-comparison test.

In vitro binding assays

The insert DNA of pGAD*HIP14*-500 was re-cloned into pGEX4T2 (Pharmacia), grown and induced with 1 mM IPTG. Cell pellets were resuspended in 5 ml of lysis buffer [150 mM NaCl, 50 mM Tris–HCl (pH 7.5), 0.5% NP40, 2.5 mM $MgCl_2$, 2.5 mM KCl, 1.5 mM $CaCl_2$, and protease inhibitor cocktail (Boehringer Mannheim)] containing 0.5 mg/ml lysozyme, sonicated and centrifuged. The resulting supernatant was bound to GST–Sepharose 4B beads (Pharmacia). To prepare htt, human embryonic kidney (HEK) 293T cells were transfected with pCI1955-15 or pCI1955-128 (38). Cell pellets were resuspended in 250 μl of HEPES buffer [10 mM HEPES (pH 8.3), 1.5 mM $MgCl_2$ and protease inhibitor cocktail], homogenized and centrifuged. 500 μg of protein was bound to beads and washed extensively. GST–HIP14 or GST-only beads were boiled in SDS sample buffer, resolved on 7.5% polyacrylamide gels and transferred to polyvinylidene difluoride (PVDF) membranes (39). The anti-htt antibody BKP1 (1 : 100) (16) was used for immunodetection.

Co-immunoprecipitation of HIP14 with htt

Twenty-five microliters per sample of protein G sepharose beads (Pharmacia) were washed four times with lysis buffer (5 mM HEPES and 1% Triton X-100) and bound to the anti-htt antibody 2166 (Chemicon), along with an antibody-omitted control. The beads were then washed and 100 μl of slurry was used for each reaction. To express htt and HIP14, HeLa cells

were co-transfected with HIP14 and htt pCI1955-15 or pCI1955-128, using FuGene 6 transfection reagent (Roche) as indicated by the manufacturer. Twenty-four hours later, cells were lysed and 400 µl of lysate (~2 mg protein) were added to the beads and incubated end-over-end at 4°C overnight. Samples were washed five times with RIPA buffer [50 mM Tris (pH 8), 150 mM NaCl, 0.1% SDS, 1% NP-40 and 0.5% deoxycholic acid], boiled in SDS sample buffer, separated on 7.5% acrylamide gels and transferred to PVDF membrane (Bio-Rad). Western blots were performed using anti-HIP14 polyclonal antibody and developed using ECL (Amersham) chemiluminescence reagent.

cDNA cloning and the identification of EST clones

Approximately 1×10^6 pfu from two human brain cDNA libraries (gifts from Drs Montal and Johnston at John Hopkins University) were screened using standard procedures (40). HIP14 cDNA from pGAD*HIP14*-500 was used as a probe. After secondary screening, all positive clones were subcloned into pBluescript SK(−) using the *in vivo* excision procedure (41).

To identify additional cDNA clones, we searched the EST database (dbEST) using a BLAST program (42) at NCBI (http://www.ncbi.nlm.nih.gov). The EST clones 41870 and 838424 were obtained from Research Genetics Inc. The entire coding region was assembled in pBluescriptII SK(−).

DNA sequencing and DNA/amino acid sequence analysis

DNA was sequenced using the ABI 373A DNA sequencer. The DNA sequence and the translated amino acid sequences were compared with sequence databases using BLASTN and BLASTP, respectively (42). The colinear alignment of the predicted amino acid sequences was performed using Pileup [Wisconsin Package Version 10.0, Genetics Computer Group (GCG), Wisconsin] and displayed using BOXSHADE (http://www.isrec.isb-sib.ch/software/BOX_form.html). The transmembrane helices were predicted by using PSORTII (http://www.genome.ad.jp), and TMpred (http://www.hgsc.bcm.tmc.edu:8088/search-launcher/launcher.html).

Chromosomal mapping of the *HIP14* gene

Chromosomal mapping of the *HIP14* gene was performed by fluorescence *in situ* hybridization (FISH) to normal human lymphocyte chromosomes counterstained with propidium iodide and 4′,6-diamidin-2-phenylindole dihydrochloride (DAPI) (43). Two *HIP14* genomic bacterial artificial chromosome (BAC) clones (44), 363B17 and 463M12, were identified. Biotinylated genomic clones were detected with avidin–fluorescein isothiocyanate (FITC). Images were captured by a thermoelectrically cooled charge-coupled device (CCD) camera (Photometrics, Tucson, AZ). Separate images of DAPI-banded chromosomes and FITC-targeted chromosomes were obtained. Pseudocolored images of the DAPI and FITC were overlaid and merged electronically (45).

Toxicity of *HIP14*

HEK293T cells were cultured and transfected with pCIneoHIP14. Toxicity was measured 48 h after $CaPO_4$ transfection using a modified MTT assay as previously described (46). htt with 128 repeats (1955-128) and a LacZ-expressing vector were used as positive and negative controls, respectively.

Northern blot analysis

Multiple human adult tissue northern blots (Clontech) were hybridized with [α-^{32}P] dCTP-labeled *HIP14*-500 or human actin cDNA in ExpressHyb hybridization solution (Clontech) at 68°C. The membranes were washed under stringent conditions (0.1 × SSC, 0.1% SDS, 55°C) and exposed to X-ray film (X-OMAT, Kodak) at −80°C with intensifying screens (DuPont).

Generation of antibodies

The generation of the htt-specific antibody BKP1 is described elsewhere (16). To generate a polyclonal antibody for HIP14 (HIP14PEP1), a peptide corresponding to amino acids 49–60 (RKTHIDDYSTWD) that represents a unique amino acid sequence was synthesized and coupled to keyhole limpet hemocyanin (KLH) (Pierce) with succinimidyl 4-(*N*-maleimidomethyl)cyclohexane-1-carboxylate (Pierce). Female New Zealand White rabbits were injected with HIP14 peptide and Freund's adjuvant. Antibody was purified using standard Thiol–sepharose affinity columns (Pharmacia).

Western blot analysis

Protein from frozen human tissues and fresh mouse tissues was isolated as stated above, denatured in SDS sample buffer, loaded onto 7.5% acrylamide SDS gel and transferred onto PVDF membranes. Western blot analysis was conducted using the purified HIP14PEP1 antibody (1 : 50), and then detected using enhanced chemiluminescence (Amersham). Equivalent protein loading was assessed by GAPDH (Chemicon) immunoblotting of the PVDF membranes.

Immunocytochemistry in neuronal precursor NT2 cells and ES cell-derived neurons

Double immunofluorescence was performed with neuronal NT2 cells and ES-cell-derived neurons. Cells were fixed in 4% (w/v) paraformaldehyde, permeabilized in PBS containing 1% paraformaldehyde and 0.3% Triton X-100 for 5 min, washed, and incubated with anti-HIP14 antibody overnight at 4°C. Slides were incubated with monoclonal antibodies (mAbs) directed against GM130 (Transduction Laboratories), β-COP (Sigma), clathrin heavy chain (Transduction Laboratories), γ-adaptin (Transduction Laboratories), calreticulin or Grp78 (StressGen, BC) in phosphate-buffered saline (PBS) and 2% normal goat serum for 2 h. Slides were then incubated with goat anti-rabbit Alexa 488 and/or goat anti-mouse Alexa 568, respectively (Molecular Probes), counterstained with propidium iodide or DAPI and mounted in Mowiol (Aldrich). Immunofluorescence was detected using a laser confocal microscope (Biorad) or conventional immunofluorescence

microscopy. Images were captured digitally with a CCD camera (Princeton Instruments Inc.).

Fluorogold injections

Injections of the fluorogold retrograde tracer were performed to label the population of projection neurons in the striatum, which are the first to degenerate in HD (47), and to determine if HIP14 was localized in these neurons. Fluorogold tracer injected into the globus pallidus is retrogradely transported to the cell body of the striatopallidal neurons in the striatum. To perform the injections, mice were anaesthetized with inhaled isofluorane and placed in a stereotaxic apparatus, and a small craniotomy was performed at the injection site. Using pulled-glass pipettes and the nanojector microinjector (World Precision Instruments), 20 nl of 1% fluorogold (Fluorochrome Inc.) in dH_2O was slowly injected (10 nl/min) into the globus pallidus (from Bregma: anterior −2.63 mm, lateral ± 1.8 mm, depth 4.33 mm at a 30° angle). Five minutes following injection, the glass pipette was slowly withdrawn and the scalp was closed with surgical sutures. The animal was given post-operative care in a heated chamber prior to returning to its home cage. After a 24 h survival time, mice were sacrificed with isofluorane and perfused intercardially with 3% paraformaldehyde. The brain was removed and allowed to fix in 3% paraformaldehyde for 24 h. Twenty-five micrometer brain sections were cut on a vibratome and then stained for HIP14 and htt (HD3 antibody) (1) using standard immunohistochemical techniques. Images were taken from either a Zeiss Axioscope or a Bio-Rad Radiance 2000 confocal imaging system.

Immunohistochemical analyses of mouse brains

To assess the expression of HIP14 *in vivo*, the brains of adult FVB/N mice were processed with either a neuron-specific antibody (NeuN, Chemicon) or an astroglial-specific marker (GFAP, Sigma) and HIP14PEP1. Mice were perfused with cold 3% paraformaldehyde in 0.1 M PBS, brains were post-fixed, and 30 µm sections were cut on a vibrating microtome (Vibratome). Sections were rinsed in 0.1 M PBS with 0.3% Tween-20, blocked (0.1% PBS with 0.3% Tween-20, 3% whole goat serum and 5% bovine serum albumin) and placed into primary antisera against HIP14PEP1 and NeuN or GFAP for 24 h at 4°C. The samples were then blocked and incubated in either 1 : 100 goat anti-rabbit CY-3 (Molecular Probes) with anti-HIP14 antibody, or 1 : 250 goat anti-mouse Alexa 488 with NeuN or GFAP. Sections were mounted on gelatin-coated slides, dehydrated by serial ethanol washes, mounted with Fluoromount (Gurr), and analyzed using a laser confocal microscope (Bio Rad). Digital images were captured on a CCD camera (Princeton Instruments Inc.), and processed into double immunofluorescence figures using the NIH-Image program.

Light and electron-microscopic level immunocytochemical analysis of mouse brains

Mice were perfused intracardially with 200 ml of 3% paraformaldehyde and 0.15% glutaraldehyde in 0.1 M phosphate buffer (PB) at pH 7.2 for electron-microscopic analysis. Brains were processed as described elsewhere (1,48). Controls included the omission of primary antisera. Following DAB visualization, some sections were osmicated [1% osmium tetroxide (OsO_4) in 0.1 M cacodylate buffer], rinsed, and stained overnight in 2% aqueous uranyl acetate.

For ultrastructural analysis, ultra-small colloidal gold conjugated secondary antibody (Aurion, Wageningen, The Netherlands) was used. Following a post-fixation with 2.5% glutaraldehyde, gold particles were intensified using the R-gent SE-EM silver enhancement kit (Aurion). Sections were further fixed with 0.5% OsO_4 in 0.1 M PB, dehydrated in ethanol and propylene oxide (1 : 1) and flat-embedded in Eponate 12 (Ted Pella, Redding, CA). Ultrathin sections (90 nm) were cut using a Leica Ultracut S ultramicrotome, and counterstained with 5% aqueous uranyl acetate for 5 min followed by lead citrate for 5 min. Thin sections were examined using a HITACHI H-7500 electron microscope. Following DAB staining, some sections were mounted for light microscopy.

Transformation of HIP14 into *akr1*Δ yeast

The entire coding region of *HIP14* was isolated from pBluescript*HIP14* and ligated to pAD5 (2µ, ADH1 promoter, LEU2). *AKR1* and *akr1*Δ yeast cells were transformed with pAD5–HIP14, pPB575 (2µ, LEU2, AKR1) (22) and pAD5. The cells were plated onto SD-leu, grown at 25°C and streak-purified twice. Random colonies were picked from each streak, and incubated at 25°C and 37°C. Colony growth and size were monitored 72 h later.

Assay of Ste3p stability

Individual colonies from the transformants above were innoculated and grown overnight, re-innoculated and grown until OD_{600} reached 0.8. Cycloheximide 10 µg/ml was added, and an aliquot removed at 'time 0' and other time-points. Protein extracts were prepared as previously described (15). Ten microliter of sample was separated on a 7.5% acrylamide gel, and transferred to PVDF membranes. The blots were immunoreacted against anti-Ste3p monoclonal antibody, and visualized using ECL (Pharmacia) as described previously (15).

ACKNOWLEDGEMENTS

We thank Michael Kalchman for originating these studies, Dr Philip Hieter for helpful discussions throughout this work, Dr Steven Sherer for the chromosomal mapping analysis and Dr Dan Gietz for providing guidance in the yeast library screens. S.G is a postdoctoral fellow in Dr Philip Hieter's laboratory. This work was funded by the Canadian Genetic Diseases Network, the Centre for Molecular Medicine and Therapeutics (CMMT), a Medical Research Council (MRC) of Canada operating grant to M.R.H., National Institutes of Health Grant NS35255 to S.M.H. and C.-A.G., and the Huntington Disease Society of America (M.M., C.-A.G., S.M.H. and M.R.H.). M.R.H is a holder of a Canada Research Chair.

REFERENCES

1. Gutekunst, C.A., Levey, A.I., Heilman, C.J., Whaley, W.L., Yi, H., Nash, N.R., Rees, H.D., Madden, J.J. and Hersch, S.M. (1995) Identification and localization of huntingtin in brain and human lymphoblastoid cell lines with anti-fusion protein antibodies. *Proc. Natl Acad. Sci. USA*, **92**, 8710–8714.
2. Trottier, Y., Devys, D., Imbert, G., Saudou, F., An, I., Lutz, Y., Weber, C., Agid, Y., Hirsch, E.C. and Mandel, J.L. (1995) Protein cellular localization of the Huntington's disease protein and discrimination of the normal and mutated form. *Nat. Genet.*, **10**, 104–110.
3. Boutell, J.M., Thomas, P., Neal, J.W., Weston, V.J., Duce, J., Harper, P.S. and Jones, A.L. (1999) Aberrant interactions of transcriptional repressor proteins with the Huntington's disease gene product, huntingtin. *Hum. Mol. Genet.*, **8**, 1647–1655.
4. Kegel, K.B., Meloni, A.R., Yi, Y., Kim, Y.J., Doyle, E., Cuiffo, B.G., Sapp, E., Wang, Y., Qin, Z.H., Chen, J.D. *et al.* (2002) Huntingtin is present in the nucleus, interacts with the transcriptional corepressor C-terminal binding protein, and represses transcription. *J. Biol. Chem.*, **277**, 7466–7476.
5. Faber, P.W., Barnes, G.T., Srinidhi, J., Chen, J., Gusella, J.F. and MacDonald, M.E. (1998) Huntingtin interacts with a family of WW domain proteins. *Hum. Mol. Genet.*, **7**, 1463–1474.
6. Nucifora, F.C. Jr, Sasaki, M., Peters, M.F., Huang, H., Cooper, J.K., Yamada, M., Takahashi, H., Tsuji, S., Troncoso, J., Dawson, V.L. *et al.* (2001) Interference by huntingtin and atrophin-1 with CBP-mediated transcription leading to cellular toxicity. *Science*, **291**, 2423–2428.
7. Steffan, J.S., Bodai, L., Pallos, J., Poelman, M., McCampbell, A., Apostol, B.L., Kazantsev, A., Schmidt, E., Zhu, Y.Z., Greenwald, M. *et al.* (2001) Histone deacetylase inhibitors arrest polyglutamine-dependent neurodegeneration in *Drosophila*. *Nature*, **413**, 739–743.
8. Metzler, M., Legendre-Guillemin, V., Gan, L., Chopra, V., Kwok, A., McPherson, P.S. and Hayden, M.R. (2001) HIP1 functions in clathrin-mediated endocytosis through binding to clathrin and adaptor protein 2. *J. Biol. Chem.*, **276**, 39271–39276.
9. Li, X.J., Li, S.H., Sharp, A.H., Nucifora, F.C., Jr, Schilling, G., Lanahan, A., Worley, P., Snyder, S.H. and Ross, C.A. (1995) A huntingtin-associated protein enriched in brain with implications for pathology. *Nature*, **378**, 398–402.
10. Li, S.H., Gutekunst, C.A., Hersch, S.M. and Li, X.J. (1998) Association of HAP1 isoforms with a unique cytoplasmic structure. *J. Neurochem.*, **71**, 2178–2185.
11. Li, Y., Chin, L-S., Levey, A.I. and Li, L. (2002) Huntingtin-associated protein-1 interacts with Hrs and functions in endosomal trafficking. *J. Biol. Chem.*, **277**, 28212–28221.
12. Bao, J., Sharp, A.H., Wagster, M.V., Becher, M., Schilling, G., Ross, C.A., Dawson, V.L. and Dawson, T.M. (1996) Expansion of polyglutamine repeat in huntingtin leads to abnormal protein interactions involving calmodulin. *Proc. Natl Acad. Sci. USA*, **93**, 5037–5042.
13. Sittler, A., Walter, S., Wedemeyer, N., Hasenbank, R., Scherzinger, E., Eickhoff, H., Bates, G.P., Lehrach, H. and Wanker, E.E. (1998) SH3GL3 associates with the huntingtin exon 1 protein and promotes the formation of polygln-containing protein aggregates. *Mol. Cell*, **2**, 427–436.
14. Boutell, J.M., Wood, J.D., Harper, P.S. and Jones, A.L. (1998) Huntingtin interacts with cystathionine β-synthase. *Hum. Mol. Genet.*, **7**, 371–378.
15. Givan, S.A. and Sprague G.F., Jr (1997) The ankyrin repeat-containing protein Akr1p is required for the endocytosis of yeast pheromone receptors. *Mol. Biol. Cell*, **8**, 1317–1327.
16. Kalchman, M.A., Graham, R.K., Xia, G., Koide, H.B., Hodgson, J.G., Graham, K.C., Goldberg, Y.P., Gietz, R.D., Pickart, C.M. and Hayden, M.R. (1996) Huntingtin is ubiquitinated and interacts with a specific ubiquitin conjugating enzyme. *J. Biol. Chem*, **271**, 19385–19394.
17. Hackam, A.S., Yassa, A.S., Singaraja, R., Metzler, M., Gutekunst, C.A., Gan, L., Warby, S., Wellington, C.L., Vaillancourt, J., Chen, N. *et al.* (2000) Huntingtin interacting protein 1 induces apoptosis via a novel caspase-dependent death effector domain. *J. Biol. Chem.*, **275**, 41299–41308.
18. Gervais, F.G., Singaraja, R., Xanthoudakis, S., Gutekunst, C.A., Leavitt, B.R., Metzler, M., Hackam, A.S., Tam, J., Vaillancourt, J.P., Houtzager, V. *et al.* (2002) Recruitment and activation of caspase-8 by the Huntingtin-interacting protein Hip-1 and a novel partner Hippi. *Nat. Cell Biol.*, **4**, 95–105.
19. Li, H., Li, S.H., Yu, Z.X., Shelbourne, P. and Li, X.J. (2001) Huntingtin aggregate-associated axonal degeneration is an early pathological event in Huntington's disease mice. *J. Neurosci.*, **21**, 8473–8481.
20. Nakamura, N., Lowe, M., Levine, T.P., Rabouille, C. and Warren, G. (1997) The vesicle docking protein p115 binds GM130, a *cis*-Golgi matrix protein, in a mitotically regulated manner. *Cell*, **89**, 445–455.
21. Kalchman, M.A., Koide, H.B., McCutcheon, K., Graham, R.K., Nichol, K., Nishiyama, K., Lynn, F.C., Kazemi-Esfarjani, P., Wellington, C.L., Metzler, M. *et al.* (1997) HIP1, a human homologue of *S. cerevisiae* Sla2p, interacts with membrane-associated huntingtin in the brain. *Nat. Genet.*, **16**, 44–53.
22. Kao, L.R., Peterson, J., Ji, R., Bender, L. and Bender, A. (1996) Interactions between the ankyrin repeat-containing protein Akr1p and the pheromone response pathway in *Saccharomyces cerevisiae*. *Mol. Cell Biol.*, **16**, 168–178.
23. Nance, M.A. (1997) Clinical aspects of CAG repeat diseases. *Brain Pathol.*, **7**, 881–900.
24. Ross, C.A. (1995) When more is less: pathogenesis of glutamine repeat neurodegenerative diseases. *Neuron*, **15**, 493–496.
25. Velier, J., Kim, M., Schwarz, C., Kim, T.-W., Sapp, E., Chase, K., Aronin, N. and DiFiglia, M. (1998) Wild-type and mutant huntingtins function in vesicle trafficking in the secretory and endocytic pathways. *Exp. Neurol.*, **152**, 34–40.
26. Feng, Y. and Davis, N.G. (2000) Akr1p and the type I casein kinases act prior to the ubiquitination step of yeast endocytosis: Akr1p is required for kinase localization to the plasma membrane. *Mol. Cell Biol.*, **20**, 5350–5359.
27. Bonifacino, J.S. and Weissman, A.M. (1998) Ubiquitin and the control of protein fate in the secretory and endocytic pathways. *Annu. Rev. Cell Dev. Biol.*, **14**, 19–57.
28. Hicke, L. (1999) Gettin' down with ubiquitin: turning off cell-surface receptors, transporters and channels. *Trends Cell Biol.*, **9**, 107–112.
29. Engelender, S., Sharp, A.H., Colomer, V., Tokito, M.K., Lanahan, A., Worley, P., Holzbaur, E.L.F. and Ross, C.A. (1997) Huntingtin-associated protein 1 (HAP1) interacts with the $p150^{Glued}$ subunit of dynactin. *Hum. Mol. Genet.*, **6**, 2205–2212.
30. Vieira, A.V., Lamaze, C. and Schmid, S.L. (1996) Control of EGF receptor signaling by clathrin-mediated endocytosis. *Science*, **274**, 2086–2089.
31. Wesp, A., Hicke, L., Palecek, J., Lombardi, R., Aust, T., Munn, A.L. and Riezman, H. (1997) End4p/Sla2p interacts with actin-associated proteins for endocytosis in *Saccharomyces cerevisiae*. *Mol. Biol. Cell*, **8**, 2291–2306.
32. Legendre-Guillemin, V., Metzler, M., Charbonneau, M., Gan, L., Chopra, V., Philie, J., Hayden, M.R. and McPherson, P.S. (2002) HIP1 and HIP12 display differential binding to F-actin, AP2, and clathrin. Identification of a novel interaction with clathrin light chain. *J. Biol. Chem.*, **277**, 19897–19904.
33. Rao, D.S., Chang, J.C., Kumar, P.D., Mizukami, I., Smithson, G.M., Bradley, S.V., Parlow, A.F. and Ross, T.S. (2001) Huntingtin interacting protein 1 is a clathrin coat binding protein required for differentiation of late spermatogenic progenitors. *Mol. Cell Biol.*, **21**, 7796–7806.
34. Mishra, S.K., Agostinelli, N.R., Brett, T.J., Mizukami, I., Ross, T.S. and Traub, L.M. (2001) Clathrin- and AP-2-binding sites in HIP1 uncover a general assembly role for endocytic accessory proteins. *J. Biol. Chem.*, **276**, 46230–46236.
35. Waelter, S., Scherzinger, E., Hasenbank, R., Nordhoff, E., Lurz, R., Goehler, H., Gauss, C., Sathasivam, K., Bates, G.P., Lehrach, H. and Wanker, E.E. (2001) The huntingtin interacting protein HIP1 is a clathrin and α-adaptin-binding protein involved in receptor-mediated endocytosis. *Hum. Mol. Genet.*, **10**, 1807–1817.
36. Gietz, R.D. and Woods, R.A. (1998) Transformation of yeast by the lithium acetate/single-stranded carrier DNA/PEG method. In Brown, A.J.P. and Tuite, M.F. (eds), *Methods in Microbiology*. Academic Press, New York, **26**, 18–26.
37. Gietz, R.D., Triggs-Raine, B., Robbins, A., Graham, K.C. and Woods, R.A. (1997) Identification of proteins that interact with a protein of interest: applications of the yeast two hybrid system. *Mol. Cell Biochem.*, **172**, 67–79.
38. Wellington, C.L., Ellerby, L.M., Hackam, A.S., Margolis, R.L., Trifiro, M.A., Singaraja, R., McCutcheon, K., Salvesen, G.S., Propp, S.S., Bromm, M. *et al.* (1998) Caspase cleavage of gene products associated with triplet expansion disorders generates truncated fragments containing the polyglutamine tract. *J. Biol. Chem.*, **273**, 9158–9167.

39. Towbin, H., Staehelin, T. and Gordon, J. (1979) Electrophoretic transfer of proteins from polyacrylamide gels to nitrocellulose sheets: procedure and some applications. *Proc. Natl Acad. Sci. USA*, **76**, 4350–4354.
40. Sambrook, J., Fritsch, E.F. and Maniatis, T. (1989) *Molecular Cloning: A Laboratory Manual*. Cold Spring Harbor Laboratory Press, Cold Spring Harbor, NY.
41. Short, J.M., Fernandez, J.M., Sorge, J.A. and Huse, W.D. (1988) Lambda ZAP: a bacteriophage lambda expression vector with *in vivo* excision properties. *Nucleic Acids Res.*, **16**, 7583–7600.
42. Altschul, S.F., Madden, T.L., Schaffer, A.A., Zhang, J., Zhang, Z., Miller, W. and Lipman, D.J. (1997) Gapped BLAST and PSI-BLAST: a new generation of protein database search programs. *Nucleic Acids Res.*, **25**, 3389–3402.
43. Lichter, P., Tang, C.J., Call, K., Hermanson, G., Evans, G.A., Housman, D. and Ward, D.C. (1990) High-resolution mapping of human chromosome 11 by *in situ* hybridization with cosmid clones. *Science*, **247**, 64–69.
44. Shizuya, H., Birren, B., Kim, U.J., Mancino, V., Slepak, T., Tachiiri, Y. and Simon, M. (1992) Cloning and stable maintenance of 300-kilobase-pair fragments of human DNA in *Escherichia coli* using an F-factor-based vector. *Proc. Natl Acad. Sci. USA*, **89**, 8794–8797.
45. Boyle, A.L., Feltquite, D.M., Dracopoli, N.C., Housman, D.E. and Ward, D.C. (1992) Rapid physical mapping of cloned DNA on banded mouse chromosomes by fluorescence *in situ* hybridization. *Genomics*, **12**, 106–115.
46. Hackam, A.S., Singaraja, R., Wellington, C.L., Metzler, M., McCutcheon, K., Zhang, T., Kalchman, M. and Hayden, M.R. (1998) The influence of huntingtin protein size on nuclear localization and cellular toxicity. *J. Cell Biol.*, **141**, 1097–1105.
47. Reiner, A., Albin, R.L., Anderson, K.D., D'Amato, C.J., Penney, J.B. and Young, A.B. (1988) Differential loss of striatal projection neurons in Huntington disease. *Proc. Natl Acad. Sci. USA*, **85**, 5733–5737.
48. Gutekunst, C.A., Li, S.H., Yi, H., Ferrante, R.J., Li, X.J. and Hersch, S.M. (1998) The cellular and subcellular localization of huntingtin-associated protein 1 (HAP1): comparison with huntingtin in rat and human. *J. Neurosci.*, **18**, 7674–7686.

doi:10.1006/geno.2002.6857, available online at http://www.idealibrary.com on IDEAL

Identification and Characterization of Novel Members of the CREG Family, Putative Secreted Glycoproteins Expressed Specifically in Brain

Ryota Kunita,[1] Asako Otomo,[2] and Joh-E Ikeda[1,2,*]

[1]SORST, Japan Science and Technology Corporation (JST), and [2]Department of Molecular Neuroscience, Institute of Medical Sciences, Tokai University School of Medicine, Isehara, Kanagawa 259-1193, Japan

*To whom correspondence and reprint requests should be addressed. Fax: +81-463-91-4993. E-mail: joh-e@nga.med.u-tokai.ac.jp.

The cellular repressor of E1A-stimulated genes, CREG, is a secreted glycoprotein that enhances differentiation of pluripotent stem cells. Here we report two novel members of the CREG family, human *CREG2* and mouse *Creg2* cDNAs. The predicted human and mouse protein sequences exhibit 35% identity with CREG protein. Northern blot analyses demonstrate specific *CREG2* and *Creg2* transcription in brain—in the case of *CREG2*, mainly in the limbic system of the brain. Both mouse and human CREG2 fused to the carboxy terminus of EGFP in NIH3T3 cells localize to the perinuclear region, which demonstrates implicit endoplasmic reticulum and Golgi localization. Human and mouse CREG2 are *N*-glycosylated in HeLa cells and deletion of amino-terminal sequences completely abolishes *N*-glycosylation, indicating that the N termini of both proteins may function as signal sequences. Thus, human and mouse CREG2 are putative secreted glycoproteins and may be novel neuronal extracellular molecules.

The cellular repressor of E1A-stimulated genes (CREG) is a secreted glycoprotein that antagonizes 12SE1A-mediated transcriptional activation of both the adenovirus E2 and cellular HSP70 promoters [1]. CREG also antagonizes E1A-mediated transformation of primary cultured rat kidney cells, inhibits transcriptional activation by E2F [1], and promotes NTERA-2 cell differentiation [2]. CREG has a functional signal sequence at its amino terminus targeting the protein into the endoplasmic reticulum (ER) and shows a localization in the perinuclear region typical for secreted proteins [2]. It has been proposed that CREG acts as an extracellular ligand through binding to a putative cell surface receptor [2]. So far, no other CREG family genes have been identified.

We have identified and characterized the ubiquitin-specific protease 17 gene, *USP17*, which is encoded by a tandem repetitive RS447 megasatellite sequence on human chromosome 4p16.1 [3–6]. To delineate the physiological role of USP17, we screened for USP17-interacting proteins. CREG2 was identified as a candidate USP17-interacting protein using yeast two-hybrid screening with a human brain cDNA library. The first *CREG2* cDNA clone isolated lacked the 5′ region encoding the amino terminus of CREG2 (which begins at nucleotide position 648; Fig. 1A). The partial predicted amino acid sequence showed a significant identity solely to CREG protein.

Complete sequence information of the coding region for CREG2 protein was achieved by 5′-RACE using cDNA libraries from human total brain and hippocampus. The *CREG2* cDNA (3201 nucleotides), comprising a single ORF of 290 amino acid residues, was isolated (Fig. 1A). We also isolated a mouse ortholog (*Creg2*) for *CREG2* by 5′-RACE using primers from an expressed sequence tag (EST) sequence (putative partial mouse *Creg2* cDNA). Three independent products encoding 288 amino acid residues were obtained (Fig. 1B). These cDNAs differ in the length of the 5′-untranslated region (UTR). Nucleotide sequences upstream of the putative first ATG codon were found to contain three in-frame stop codons (Fig. 1B). Moreover, the flanking sequence of this ATG conforms to Kozak's rule (Fig. 1B) [7]. Thus, it is likely that the murine *Creg2* cDNAs contain an entire ORF. We identified human CREG2 cDNAs that carry no in-frame stop codons upstream of the putative first ATG codon, whose flanking sequence conforms to Kozak's rule [7]. The nucleotide sequence conservation between human and mouse cDNA sequences upstream of the ATG codons is relatively low (64%) compared with that downstream of the ATG codons (82%; data not shown). Therefore, it is still likely that human cDNA also contains an entire ORF.

Human CREG2 shows 83% amino acid identity to mouse CREG2, and these CREG2 proteins show approximately 35% identity to human, mouse, and *Drosophila* CREG proteins (Fig. 1C). Like CREG, human and mouse CREG2 amino acid sequences show no significant homology to any other protein sequences. They also contain no specific sequence motif except for the potential *N*-glycosylation consensus sequences. Despite the *CREG* genes being well conserved among a wide variety of eukaryotes, no organisms were shown to have more than a single copy of a CREG-related gene. Our sequence data show that mouse and human *CREG2* are novel members of the *CREG* family. The results of northern blot analysis indicate that both of our human and mouse cDNAs lack some parts of the transcripts. However, the sequence data derived

GENOMICS Vol. 80, Number 5, November 2002

0888-7543/02 $35.00

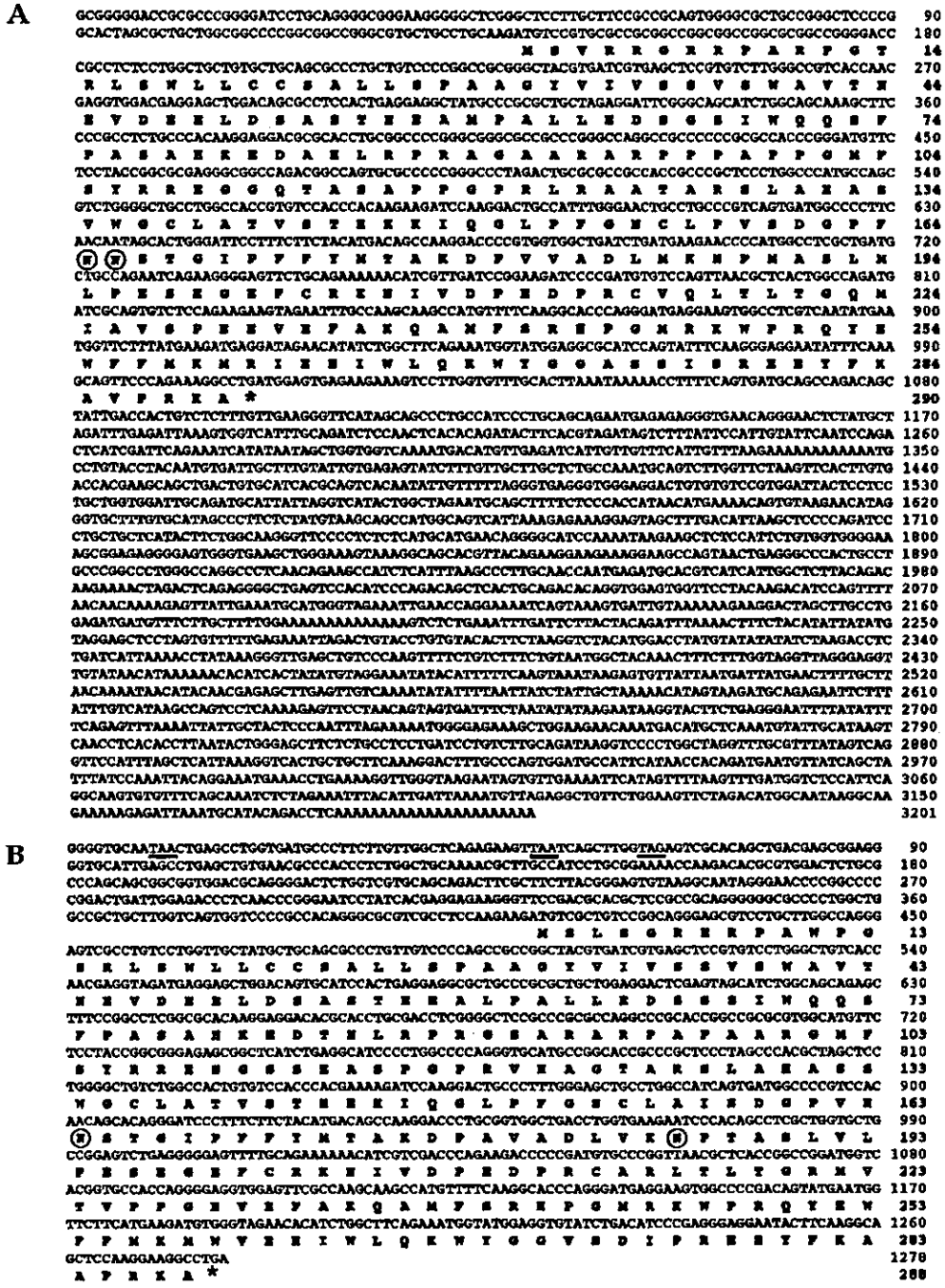

FIG. 1. Nucleotide and deduced amino acid sequences of *CREG2* and *Creg2* cDNAS and multiple alignment.(A) Nucleotide sequence of the *CREG2* cDNA and the deduced amino acid sequence. The human *CREG2* cDNA was obtained by 5′-RACE using cDNA libraries from human total brain and hippocampus (Clontech) in conjunction with the Expand Long Template PCR system (Roche). The PCR reaction was done with primers designed from the original partial cDNA cloned by a two-hybrid screening. The ORF encodes 290 amino acid residues (nucleotide position 139–1011). The downstream in-frame stop codon (TGA) is marked by an asterisk. Two potential *N*-glycosylation sites are surrounded by circles. This sequence has been deposited with the DDBJ/EMBL/GenBank database under accession number AB046109. (B) Nucleotide sequence of mouse *Creg2* cDNA and the deduced amino acid sequence. Mouse *Creg2* cDNA was obtained by 5′-RACE using a cDNA library from mouse total brain (Clontech) with primers designed from sequence information of an EST (acc. no. AW048995), a partial cDNA for *Creg2*. The ORF encodes 288 amino acid residues (nucleotide positions 412–1278). The three upstream in-frame stop codons (TAA, TAA, TAG) are underlined. The downstream in-frame stop codon (TGA) is marked by an asterisk. Two potential *N*-glycosylation sites are surrounded by circles. This sequence has been deposited with DDBJ/EMBL/GenBank database under accession number AB046110. (C) (*next page*) Multiple sequence alignment of amino acid sequences from human and mouse CREG2, human CREG (acc. no. AF084523), mouse CREG (acc. no. AF084524), and *Drosophila* CREG (acc. no. AF084522). Conserved residues are marked with white letters in black boxes and conservative substitutions are marked with shaded boxes.

doi:10.1006/geno.2002.6857, available online at http://www.idealibrary.com on IDEAL

C

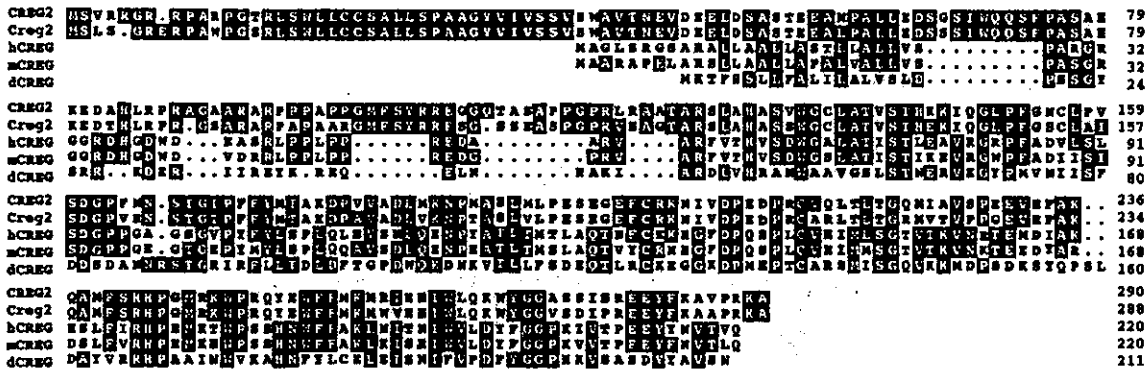

from multiple ESTs in the database and our 3′-RACE results suggest that the cDNAs lack a portion of the 3′-UTR (data not shown).

To investigate the tissue distribution of *CREG2* mRNA, human northern blots were probed with *CREG2* coding sequence. Two major transcripts of 2.6 kb and 7.0 kb were specifically detected in adult brain and were undetectable in heart, liver, pancreas, placenta, or lung (Fig. 2A). In human fetal tissues, the *CREG2* transcripts were also detectable only in brain (data not shown). We next investigated the expression of *CREG2* within the adult human central nervous system. The same major transcripts were also found mainly in the limbic system of the brain (that is, cerebral cortex, amygdala, hippocampus, and thalamus) and faintly in the spinal cord, but not in the cerebellum (Figs. 2B and 2C). These results show that unlike the CREG gene (which is ubiquitously expressed), human *CREG2* is expressed specifically in brain, especially in the limbic system. In the case of mouse *Creg2*, a 5.5-kb transcript was detected only in brain. No *Creg2* transcripts were found in heart, spleen, lung, liver, skeletal muscle, or kidney (Fig. 2D). Thus, both human and mouse genes are expressed specifically in brain.

The expression plasmids encoding C-terminally enhanced green fluorescent protein (EGFP) fused to human or mouse CREG2 or mouse CREG (a secreted glycoprotein) proteins were transfected into NIH3T3 cells to investigate subcellular localization. Similar perinuclear fluorescence was observed for human or mouse CREG2 and mouse CREG fusion proteins, implying that both human and mouse CREG2 are secreted proteins.

Given that post-translational glycosylation is a feature for most secreted proteins, we next examined whether CREG2 protein is glycosylated. HeLa cells were transfected with the expression plasmids encoding C-terminally Myc-tagged mouse or human CREG2. Western blot analysis with anti-Myc tag

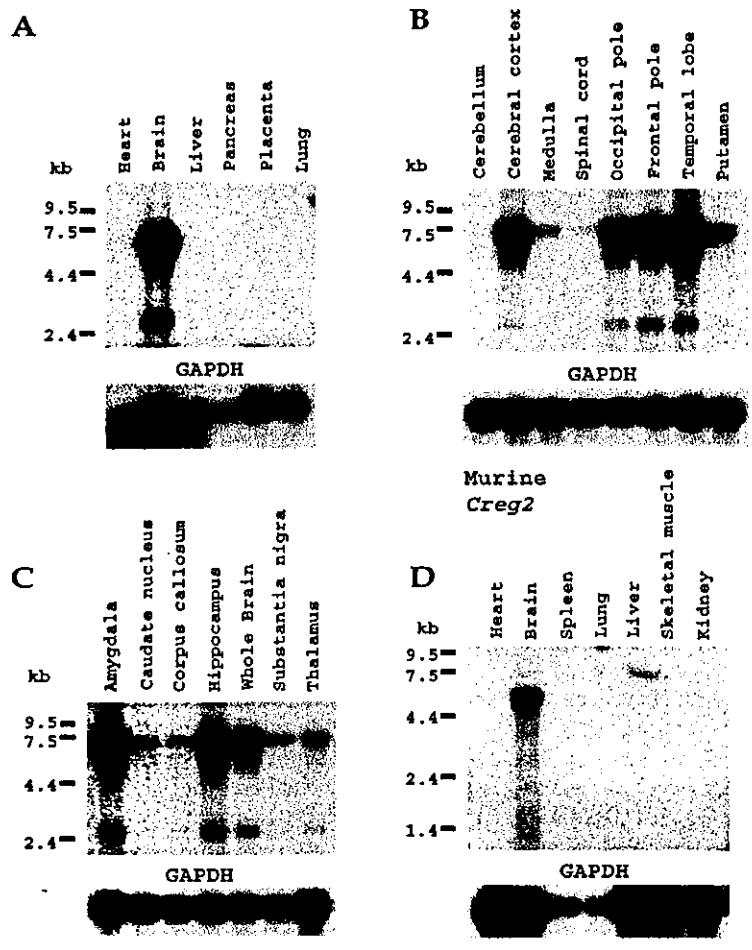

FIG. 2. Northern blot analysis of *CREG2* and *Creg2* transcripts. Human Normal Tissue Type Blot I (A) (Gene Hunter, TOYOBO), Human Brain MTN Blot II (B) (Clontech), Human Brain MTN Blot IV (C) (Clontech), and Mouse MTN Blot (D) (Clontech) were hybridized with the ^{32}P-labeled human *CREG2* entire ORF (A, B, C) or mouse *Creg2* entire ORF probes (D). After dehybridization, all membranes were rehybridized with ^{32}P-labeled human glyceraldehyde 3-phosphate dehydrogenase (*GAPDH*) cDNA (A, B, C) or mouse *Gapdh* cDNA probes (D) to confirm RNA quality and relative amounts loaded.

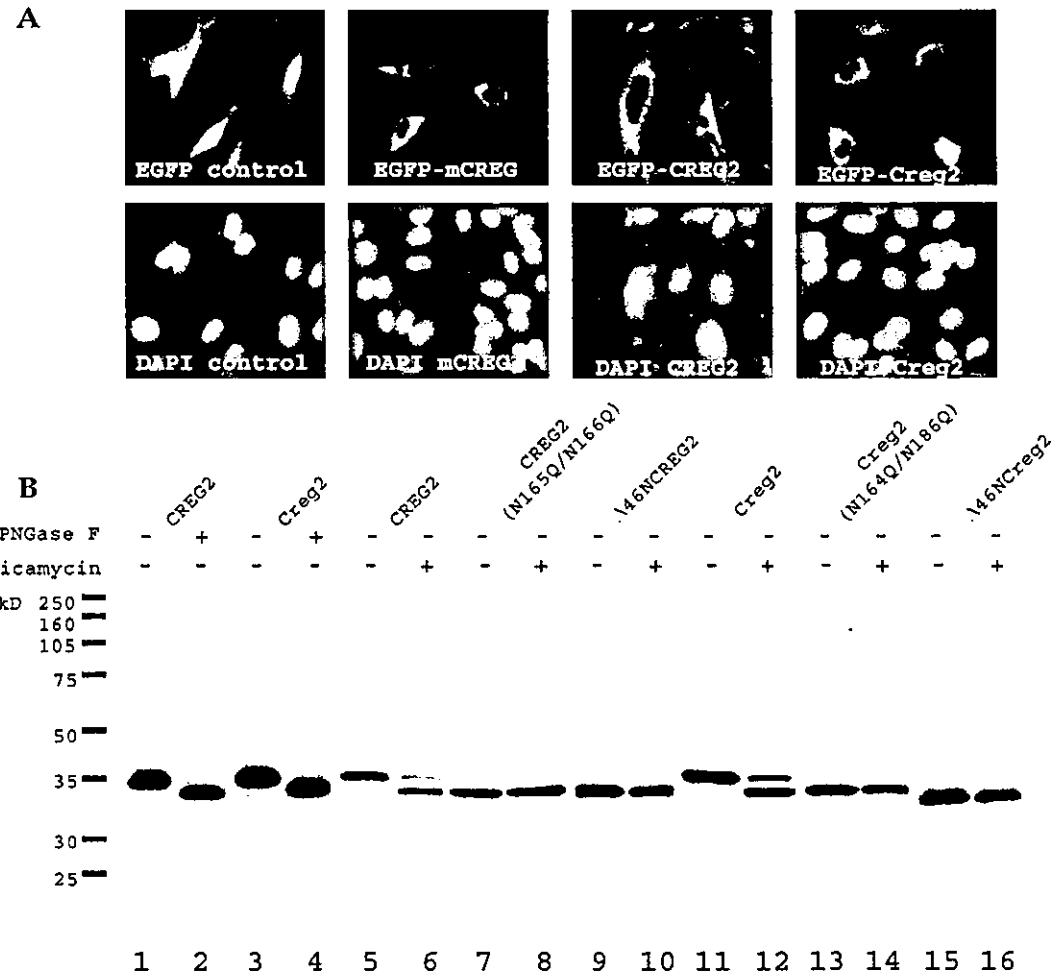

FIG. 3. Subcellular localization and *N*-glycosylation of human and mouse CREG2 in cultured cells. (A) Subcellular localization of human and mouse CREG2 and mouse CREG in NIH3T3 cells. NIH3T3 cells were transiently transfected using LipofectAMINE PLUS Reagent (Invitrogen) with the expression plasmids encoding human and mouse CREG2 or mouse CREG as indicated; all proteins are expressed as C-terminally EGFP-fused proteins. After 24 hours, cells were fixed, permeabilized, and counterstained with 4′,6-diamidino-2-phenulindole (DAPI) to visualize nuclei (bottom). (B) *N*-Glycosylation of human and mouse CREG2. HeLa cells were transiently transfected with the expression plasmids as indicated; all proteins are expressed as C-terminally Myc-tagged proteins. After 48 hours, total cell extracts were recovered from the cells transfected with the expression plasmids encoding human CREG2 (lanes 1, 2, 5, 6), mouse CREG2 (lanes 3, 4, 11, 12), human CREG2(N165Q/N166Q) (lanes 7, 8), mouse CREG2(N164Q/N186Q) (lanes 13, 14), human Δ46NCREG2 (lanes 9, 10), or mouse Δ46NCREG2 (lanes 15, 16). The cell extracts were incubated with PNGase F (lanes 2, 4) according to the manufacturer's protocol (TaKaRa). The tunicamycin (lanes 6, 8, 10, 12, 14, 16) or vehicle, DMSO (lanes 5, 7, 9, 11, 13, 15), was added to the cell culture (20 μg/ml) 12 hours before harvesting the cells. Western blot analysis was performed with an anti-Myc antibody (MBL) using the Enhanced Chemiluminescence (ECL) detection system (Amersham).

antibody (MBL) of total extracts from those cells revealed a molecular mass of 34 kDa for both human and mouse CREG2 (Fig. 3B). Treatment with peptide-*N*-glycosidase F (PNGase F) of extract from cells transfected with either Myc-tagged human CREG2 or mouse CREG2 expression plasmids shifted the higher molecular mass form (~ 34 kDa) to a smaller form (~ 32 kDa; Fig. 3B). Treatment of HeLa cells with tunicamycin, a *N*-glycosylation inhibitor, showed the same effect (Fig. 3B). These observations suggest that both human and mouse CREG2 are *N*-glycosylated. N165 and N166 of human CREG2 and N164 and N186 of mouse CREG2 are potential *N*-glycosylation sites.

To confirm *N*-glycosylation, the expression plasmids encoding the Myc-tagged mouse or human CREG2 proteins, whose two potential asparagine residues were mutated into glutamine residues, were next transfected into HeLa cells. The CREG2(N165Q/N166Q) and Creg2(N164Q/N186Q) mutant proteins were not *N*-glycosylated (Fig. 3B). In the case of mouse CREG2, two additional expression plasmids encoding the Myc-tagged Creg2N164Q or Creg2N186Q (one of two potential asparagine residues was mutated) were transfected. Only Creg2N164Q failed to be *N*-glycosylated with Creg2N186Q, showing *N*-glycosylation similar to wild-type mouse CREG2

doi:10.1006/geno.2002.6857, available online at http://www.idealibrary.com on IDEAL

protein (data not shown). These results indicate that N164 of mouse CREG2, which is only conserved in human and mouse proteins, is *N*-glycosylated. Human CREG2 is also most likely to be *N*-glycosylated on either N165 or N166, as both human and mouse proteins reveal approximately same molecular masses on the western blot analysis (Fig. 3B).

To examine whether the N termini act as functional signal sequences for entry into the ER, expression plasmids encoding proteins lacking the first 46 residues, Δ46NCREG2 or Δ46NCreg2, were transfected into HeLa cells. Notably, Δ46NCREG2 and Δ46NCreg2 proteins no longer seem to be *N*-glycosylated (Fig. 3B). These results suggest that human and mouse CREG2 have N-terminal signal sequences that are necessary for entry into the ER, where most of secreted proteins are glycosylated. Mouse CREG is also *N*-glycosylated and has a 31-amino-acid signal sequence at the N terminus under our experimental conditions (data not shown), which is consistent with reported results [2]. Δ46NCREG2 and Δ46NCreg2 migrated slightly faster than wild-type proteins treated with PNGase F on the western blots (Fig. 3B). The signal sequences of wild-type proteins were cleaved and de-*N*-glycosylated by PNGase F treatment. Therefore, functional signal sequences of CREG2 proteins might be slightly shorter than 46 amino acid residues.

We have described here two novel members of the CREG family, human and mouse CREG2. The predicted amino acid sequences show low but significant overall sequence similarity to CREG, except the sequences in the N termini (Fig. 1C). A database search indicated that human *CREG2* is located on human chromosome 2q11.2, due to the fact that the 3′ portion of the cDNA sequence shows perfect identity to the genomic sequence of the 2q11.2 region. Because the genomic sequence of this region has not been completely released, the exon/intron structures of *CREG2* are unknown. Mouse and human CREG2 localize to the perinuclear region, as does mouse CREG, suggesting ER and Golgi localization. We have shown the *N*-glycosylation of mouse and human CREG2 in HeLa cells to be absolutely dependent on their N-terminal putative signal sequences. Mouse and human CREG2 can be secreted, however, further analysis is required with antibodies against CREG2 to examine whether endogenous proteins are indeed *N*-glycosylated and secreted. *CREG2* is expressed mainly in the limbic system (that is, hippocampus, amygdala, and thalamus). Although the biological significance of CREG2 is currently unknown, the protein may have a role in brain. Given that CREG2 behaves like CREG, which inhibits cell growth and/or enhances differentiation of pluripotent cells, CREG2 may play a role in survival of neuronal cells by maintaining differentiation status, and preventing neurons from reentering the cell cycle [8]. The fact that *CREG2* and *Creg2* show similar brain-specific expression patterns indicates functional conservation. *Creg2*-mutant mice might therefore be useful in the investigation of CREG2 *in vivo* physiological function. Furthermore, the promoter sequence of *CREG2* may be used as a tool to achieve ectopic expression of the transgenes in the limbic system.

Finally, although mouse and human CREG2 may be secreted glycoproteins, cotransfection experiments with the CREG2 and USP17 expression plasmids suggest that USP17 strongly stabilizes CREG2 in a USP17 deubiquitinating activity dependent manner (R.K. *et al.*, unpublished data). Further investigation regarding whether CREG2 is a bona fide substrate for USP17 and whether the ubiquitinated CREG2 is deubiquitinated by USP17 is currently underway.

Acknowledgments

We thank Shinji Hadano, Hitoshi Osuga, and Hideo Ota (Tokai University School of Medicine) for commentary and Alex Mackenzie (Children's Hospital of Eastern Ontario Research Institute) for proofreading. Part of this work was supported by a Grant-in-Aid for Scientific Research on Priority Areas (C)–Advanced Brain Science Project from Ministry of Education, Culture, Sports, Science, and Technology, Japan.

RECEIVED FOR PUBLICATION JUNE 18;
ACCEPTED SEPTEMBER 20, 2002.

References

1. Veal, E., Eisenstein, M., Tseng, Z. H., and Gill, G. (1998). A cellular repressor of E1A-stimulated genes that inhibits activation by E2F. *Mol. Cell. Biol.* **18:** 5032–5041.
2. Veal, E., Groisman, R., Eisenstein, M., and Gill, G. (2000). The secreted glycoprotein CREG enhances differentiation of NTERA-2 human embryonal carcinoma cells. *Oncogene* **19:** 2120–2128.
3. Kogi, M., Fukushige, S., Lefevre, C., Hadano, S., and Ikeda, J.-E. (1997). A novel tandem repeat sequence located on human chromosome 4p: Isolation and characterization. *Genomics* **42:** 278–283.
4. Gondo, Y., *et al.* (1998). Human megasatellite DNA RS447: Copy-number polymorphisms and inter species conservation. *Genomics* **54:** 39–49.
5. Saitoh, Y., *et al.* (2000). The RS447 human megasatellite tandem repetitive sequence encodes a novel deubiquitinating enzyme with a functional promoter. *Genomics* **67:** 291–300.
6. Okada, T., *et al.* (2002). Unstable transmission of the RS447 human megasatellite tandem repetitive sequence that contains the *USP17* deubiquitinating enzyme gene. *Hum. Genet.* **110:** 302–313.
7. Kozak, M. (1987). An analysis of 5′-noncoding sequences from 699 vertebrate messenger RNAs. *Nucleic Acids Res.* **15:** 8125–8148.
8. Elshamy, W. M., Fridvall, L. K., and Ernfors, P. (1998). Growth arrest failure, G1 restriction point override, and S phase death of sensory precursor cells in the absence of neurotrophin-3. *Neuron* **21:** 1003–1015.

PAPER

Multiple regional ^{1}H-MR spectroscopy in multiple system atrophy: NAA/Cr reduction in pontine base as a valuable diagnostic marker

H Watanabe, H Fukatsu, M Katsuno, M Sugiura, K Hamada, Y Okada, M Hirayama, T Ishigaki, G Sobue

J Neurol Neurosurg Psychiatry 2004;**75**:103–109

See end of article for authors' affiliations

Correspondence to: Gen Sobue, MD, Department of Neurology, Nagoya University Graduate School of Medicine, Nagoya 466-8550 Japan; sobueg@med.nagoya-u.ac.jp

Received 20 December 2002
In revised form 31 March 2003
Accepted 17 May 2003

Objective: We performed ^{1}H-MR spectroscopy (^{1}H-MRS) on multiple brain regions to determine the metabolite pattern and diagnostic utility of ^{1}H-MRS in multiple system atrophy (MSA).
Methods: Examining single voxels at 3.0 T, we studied metabolic findings of the putamen, pontine base, and cerebral white matter in 24 MSA patients (predominant cerebellar ataxia (MSA-C), n=13), parkinsonism (MSA-P), n=11), in 11 age and duration matched Parkinson's disease patients (PD) and in 18 age matched control subjects.
Results: The *N*-acetylaspartate to creatine ratio (NAA/Cr) in MSA patients showed a significant reduction in the pontine base ($p<0.0001$) and putamen ($p=0.02$) compared with controls. NAA/Cr in cerebral white matter also tended to decline in long standing cases. NAA/Cr reduction in the pontine base was prominent in both MSA-P ($p<0.0001$) and MSA-C ($p<0.0001$), and putaminal NAA/Cr reduction was significant in MSA-P ($p=0.009$). It was also significant in patients who were in an early phase of their disease, and in those who showed no ataxic symptoms or parkinsonism, or did not show any MRI abnormality of the "hot cross bun" sign or hyperintense putaminal rims. NAA/Cr in MSA-P patients was significantly reduced in the pontine base ($p=0.001$) and putamen ($p=0.002$) compared with PD patients. The combined ^{1}H-MRS in the putamen and pontine base served to distinguish patients with MSA-P from PD more clearly.
Conclusions: ^{1}H-MRS showed widespread neuronal and axonal involvement in MSA. The NAA/Cr reduction in the pontine base proved highly informative in the early diagnosis of MSA prior to MRI changes and even before any clinical manifestation of symptoms.

Multiple system atrophy (MSA) is a sporadically occurring neurodegenerative disease that presents parkinsonism, cerebellar ataxia, autonomic failure, and pyramidal signs of varying severity during the course of illness.[1–3] Neuropathological findings consist of a varying neuronal loss, gliosis, and demyelination with widespread regional involvement, particularly including the striatonigral, olivopontocerebellar, and autonomic nervous systems.[4–6] The tempo and progression of multiple system involvement vary widely among individual MSA patients and have been closely related to both functional deterioration and prognosis by clinical evaluation.[7] Thus, assessing the multi-regional involvement in MSA is essential for accurate diagnosis, counselling of patients and families, optimal management of symptoms, and the usefulness of future therapeutic trials.

Proton magnetic resonance spectroscopy (^{1}H-MRS) is a valuable non-invasive MR technique for monitoring brain metabolism in vivo.[8–18] The major peaks of the ^{1}H-MRS spectrum, corresponding to *N*-acetylaspartate (NAA), creatine (Cr), and choline (Cho) containing phospholipids, have been used to evaluate neuronal loss and active myelin breakdown. The ratio of NAA to Cr (NAA/Cr) is considered a metabolic marker reflecting the functional status of neurones and axons in the brain, with a decrease indicating neuronal or axonal loss or dysfunction. Previous studies using ^{1}H-MRS in MSA with predominant parkinsonism (MSA-P) reported a significant NAA/Cr reduction in the striatum compared with Parkinson's disease (PD) patients and normal subjects.[11–14] However, the pontine base and cerebral white matter, which are also pathologically involved in MSA, have not been fully assessed by ^{1}H-MRS. Recent technical innovations have permitted ^{1}H-MRS at higher magnetic field strengths.[19–21] Multi-regional data can be obtained from single voxel ^{1}H-MRS within a short examination time with increasing signal to noise ratio (SNR).

Our purpose was to assess the extent of multiple system involvement in patients with MSA by using multiple regional single voxel ^{1}H-MRS including the putamen, pontine base, and cerebral white matter (CWM), and to further assess the diagnostic value of the regional ^{1}H-MRS.

METHODS

All patients and control subjects gave written informed consent. The MR protocol was approved by the Ethics Committee of the Nagoya University School of Medicine. Twenty four patients with MSA (12M, 12F; mean (SD) age 61 (7) years old), 11 patients with PD (5M, 6F; 63 (9) years old), and 18 control subjects with no history of any neurological disease (10M, 8F; 59 (7) years old) were studied. No significant differences in male to female ratio or age were noted among the three groups. The duration from initial

Abbreviations: Cho, choline; Cr, creatine; CWM, cerebral white matter; HCB, "hot cross bun"; HPR, hyperintense rim; MRI, magnetic resonance imaging; MRS, magnetic resonance spectroscopy; MSA, multiple system atrophy; MSA-C, multiple system atrophy with cerebellar ataxia predominant; MSA-P, multiple system atrophy with parkinsonism predominant; NAA, *N*-acetylaspartate; PD, Parkinson's disease; SNR, signal to noise ratio; VOI, volume of interest.

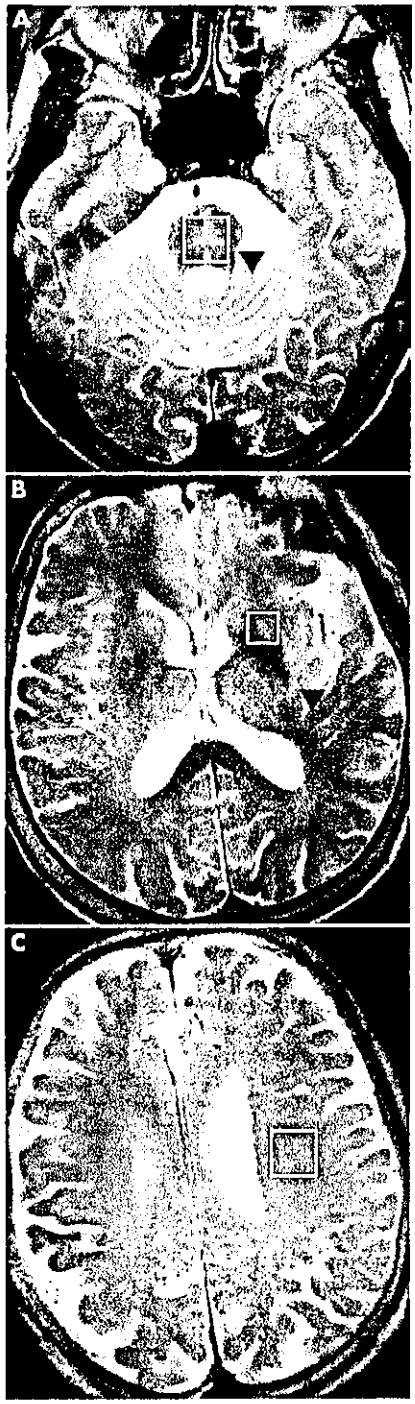

Figure 1 Location of volumes of interest are shown by squares in the pontine base (A), putamen (B), and white matter of the frontal lobe (C). Additionally, in these images, an HCB sign is present in the pons (A), as is a hyperintense putaminal rim (B). Axial T2 weighted images (3.0 T; TR: 3970, TE: 80), with respective findings are indicated by arrowheads.

symptoms to MRI and MRS evaluation also showed no differences between MSA and PD patients (MSA; 3.7 (2.4) years; PD; 4.4 (2.2) years, $p>0.4$). Diagnoses of all MSA and PD patients were "probable" according to established diagnostic criteria.[3 22] As for subtypes of MSA, cerebellar dysfunction (MSA-C) predominated in 13 patients and parkinsonism (MSA-P) in 11. We classified patients into two groups according to the presence of parkinsonian signs in MSA, based on the consensus statement for MSA diagnosis. Patients with bradykinesia plus at least one sign of either rigidity, postural instability, or tremor were considered to manifest parkinsonism and designated as "parkinsonism+", while others were taken to be "parkinsonism−". As for cerebellar dysfunction, patients with gait ataxia plus at least one sign of ataxic dysarthria, limb ataxia, or sustained gaze evoked nystagmus were considered "ataxia+", and others as "ataxia−" based on the consensus criteria.[3] Six of nine MSA-P patients and all PD patients were taking medication for parkinsonism (benserazide/levodopa 25/100 mg, or carbidopa/levodopa 10/100 mg, two or three times daily). All PD patients showed a good response to treatment.

MRI and ^{1}H-MRS were performed with a 3.0 T system (Bruker, Ettlingen, Germany) using a standard head coil with circular polarisation. The imaging protocol consisted of sagittal T1 weighted spin echo sequences (repetition time (TR), 460 ms; echo time (TE), 14 ms) and transverse T2 weighted sequences (TR, 3970 ms; TE, 80 ms). Slice thickness was 6 mm with a 1.2 mm gap and a 512×384 matrix. We evaluated whether a "hot cross bun" (HCB) sign was present in the pons and whether the putamen showed a hyperintense rim (HPR), according to the criteria described in previous reports (fig 1A, B).[7 23–26] The spectroscopic volume of interest (VOI) was placed in the pontine base (2.2 to 3.4 cm^3), the putamen (1 cm^3), and the CWM (3.4 cm^3; fig 1A to C). Voxel size was chosen to be as small as possible while maintaining an acceptable SNR in order to minimise the partial volume effect. Care was taken not to incorporate cerebrospinal fluid spaces within a VOI. The VOI in the putamen was placed on the more affected side, and the frontal lobe VOI was ipsilateral to the putaminal VOI. ^{1}H-MR spectra were acquired using a point resolved spectroscopy sequence with chemical shift selective water suppression. Spectral parameters were as follows: TR: 2000 ms; TE: 30 ms; averages: 256 in the putamen, and 64 each in the centrum semiovale and pons; data points: 1024. A shimming procedure focused on the water signal was performed to obtain a uniform and homogenous magnetic field. After Fourier transformation and zero order phase correction, relative metabolite concentrations for NAA at 2.0 ppm, Cr at 3.0 ppm, and Cho at 3.2 ppm were determined by Lorentzian curve fitting of the corresponding resonance in the frequency spectra. The baseline was corrected for purposes of data presentation. From these data, the metabolite ratios NAA/Cr, and Cho/Cr were determined as semiquantitative values. Post-procedural processing was performed by the same radiologist (HF). All preconditioning, spectroscopic measurements, and processing were performed with Paravision 2.01 software (Bruker). Total examination time including MRI and ^{1}H-MRS was <1 hour. One MSA-C patient with severe pontine atrophy was excluded because a good pontine spectrum could not be obtained.

Values obtained were entered into a database for further statistical analysis. The Mann-Whitney U test and the Kruskal-Wallis test for nonparametric statistics were performed as appropriate. When the Kruskal-Wallis test indicated differences among groups, in a multiple comparison analysis, Scheffé's test was used to identify which group differences accounted for the significant p value. Relationships of NAA/Cr reduction to duration of illness were analysed using Pearson's correlation coefficient. Calculations were performed using the Stat View statistical software package (Abacus Concepts, Berkeley, CA, USA). Statistical significance was defined as $p<0.05$.

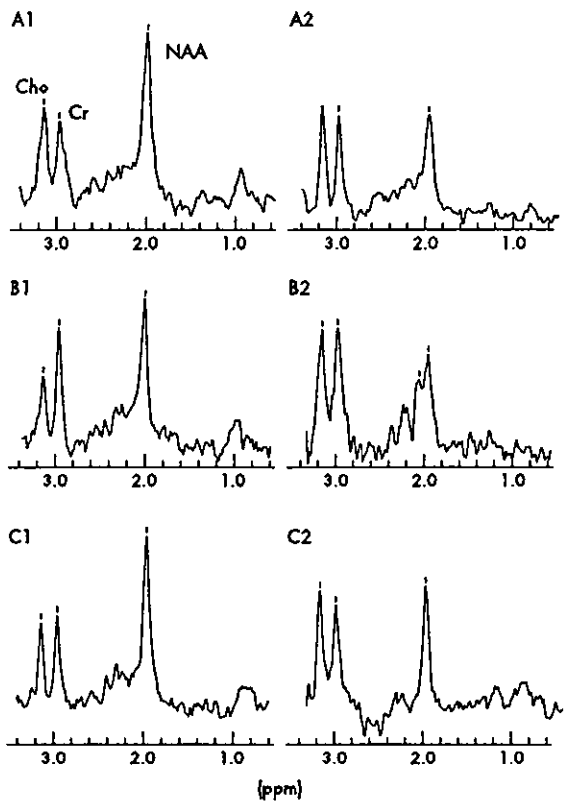

Figure 2 Representative ^{1}H-MRS spectra from control and MSA subjects. A1, B1, and C1 represent spectra from a control subject's pontine base, putamen, and cerebral white matter, respectively. A2, B2, and C2 represent spectra from those same three regions in an MSA patient. NAA, *N*-acetylaspartate; Cho, choline; Cr, creatine; MSA, multiple system atrophy; CWM, cerebral white matter.

RESULTS

Widespread NAA/Cr reduction in MSA in multiple regional ^{1}H-MRS

A representative MSA patient (fig 2) showed a marked reduction of the NAA peak in the pontine base, putamen, and cerebral white matter compared with controls. NAA/Cr was significantly reduced in the pontine base of MSA patients ($p<0.0001$) and in the putamen ($p = 0.02$) compared with controls. MSA patients also showed a lower NAA/Cr in cerebral white matter than controls, but this difference was not statistically significant ($p = 0.12$). Cho/Cr was only slightly increased in MSA, and no significant differences were found among the three groups for the pontine base, putamen, and CWM.

Prominent NAA/Cr reduction in pontine base in both MSA-C and MSA-P

Significant reductions of NAA/Cr were evident in the pontine base, putamen, and CWM in MSA-C and MSA-P compared with controls (fig 3A–C). MSA-C patients showed a significant reduction of NAA/Cr in the pontine base ($p<0.0001$) and CWM ($p = 0.02$), but not in the putamen. MSA-P patients showed a significant reduction of NAA/Cr in the pontine base ($p<0.0001$) and putamen ($p = 0.009$) but not in the CWM. These observations indicate that the NAA/Cr reduction in the pontine base was significant in both MSA-C and MSA-P. Cho/Cr was not changed in MSA-P or MSA-C compared with controls.

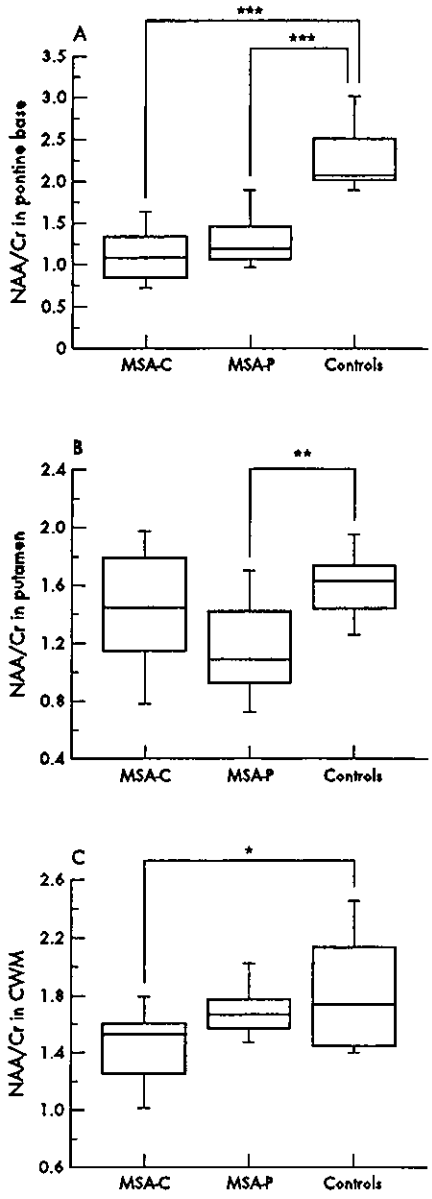

Figure 3 Box and whisker plot of the NAA/Cr ratio. Horizontal lines indicate median values. Boxes extend from the 25th to the 75th percentile. A, B, and C respectively show NAA/Cr in the pontine base, putamen, and cerebral white matter, comparing MSA-C, MSA-P, and control subjects. *$p = 0.02$, **$p = 0.009$, and ***$p<0.0001$ by Scheffé's test, respectively. NAA, *N*-acetylaspartate; Cr, creatine; Cho, choline containing component; MSA-C, multiple system atrophy with cerebellar ataxia predominant; MSA-P, multiple system atrophy with parkinsonism predominant.

Relation of NAA/Cr reduction in pontine base with disease phase, motor symptoms and MRI abnormalities in MSA

In terms of disease duration, the NAA/Cr reduction was most significant in the pontine base of patients with MSA even in an early phase of illness (fig 4). A tendency toward an inverse

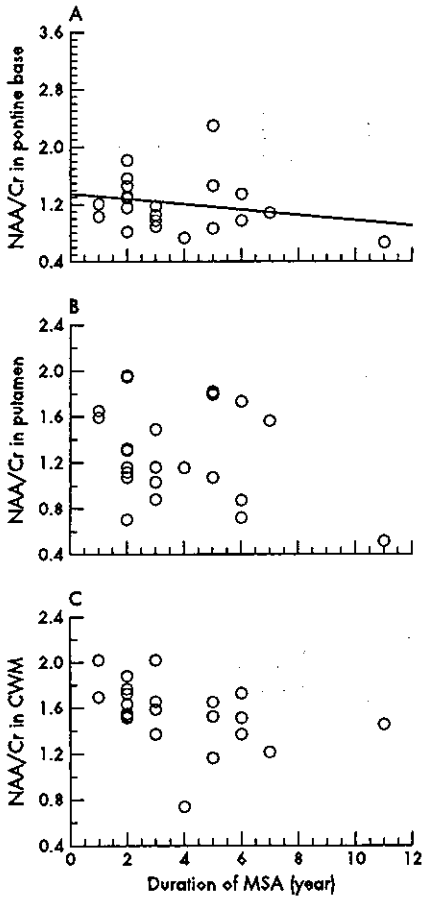

Figure 4 Correlation with duration of MSA of individual NAA/Cr ratios in the pontine base (A), putamen (B), and cerebral white matter (C). The shaded area corresponds to the mean (SD) of NAA/Cr in control subjects. NAA, *N*-acetylaspartate; Cr, creatine; CWM, cerebral white matter; MSA, multiple system atrophy.

relationship between disease duration and NAA/Cr in the three regions was observed, but did not attain significance (pontine base: $r = -0.24$, $p = 0.29$; putamen: $r = -0.32$, $p = 0.14$; CWM: $r = -0.41$, $p = 0.06$). NAA/Cr in the pontine base was significantly reduced compared with controls even in patients who did not show ataxic symptoms ($p = 0.0006$, fig 5A-1). However, NAA/Cr in the putamen and white matter was not reduced in patients with ataxia (fig 5B-1, C-1). NAA/Cr in the putamen was markedly decreased in MSA patients with parkinsonism ($p = 0.02$, Fig 5B-2), whereas patients without it exhibited no significant reduction compared with controls. NAA/Cr reduction in the pontine base, on the other hand, was significant ($p<0.0001$) irrespective of parkinsonism (Fig 5A-2).

The MRI revealed the HCB sign in the pontine base in eleven MSA patients (46%) and the HPR sign in six (25%). A significant reduction of NAA/Cr was seen in the pontine base even in patients without ($p<0.0001$) as well as in those with an HCB sign ($p<0.0001$; fig 5A-3). In the putamen and cerebral white matter, NAA/Cr values did not show any significant difference irrespective of the HCB sign (fig 5B-3, C-3). Moreover, NAA/Cr significantly decreased in the pontine base in patients both with and without HPR (fig 5A-4). NAA/Cr in the putamen and cerebral white matter did not show any significant differences irrespective of HPR signs (fig 5B-4, C-4). Cho/Cr had no significant relationship to ataxic, parkinsonism, or MRI abnormalities.

NAA/Cr in pontine base in MSA-P and PD

NAA/Cr reduction in the pontine base was highly significant in patients with MSA-P compared with both controls and PD ($p<0.0001$, $p = 0.001$; fig 6A). NAA/Cr in the putamen in MSA-P patients also showed a significant decrease compared with both controls and PD ($p = 0.003$, $p = 0.002$; fig 6B). No significant differences in NAA/Cr were noted in cerebral white matter between MSA-P and PD. These data indicate that the NAA/Cr reduction in the pontine base is a valuable marker to discriminate MSA-P from PD. In addition, combining individual NAA/Cr values for the pontine base and putamen further reduced the overlap between MSA-P and PD (fig 6D), suggesting that a combined assessment of the pontine base and putamen was more effective in discriminating between MSA-P and PD than individual area assessments. Cho/Cr did not display any significant changes in the pontine base, putamen or cerebral white matter.

DISCUSSION

We demonstrated widespread NAA/Cr reduction in the pontine base, putamen and in some cases, in the cerebral hemisphere, but no significant Cho/Cr alteration in patients with MSA using localised ^{1}H-MRS at 3.0 T. In this study, absolute metabolite concentrations were not measured. However, the specific conditions that may change the total Cr signal, such as trauma, hyperosmolar conditions, hypoxia, stroke, and tumours, were not included. Age was matched among MSA, PD, and control groups. Moreover, quantitative studies did not show significant Cr changes between MSA patients and control subjects.[11 16] Thus, the reduction of the NAA/Cr ratio in the present study can be considered due to a selective decrease in NAA levels.

NAA has been immunohistochemically demonstrated to localise almost exclusively within neurones and axons,[27 28] but some in vitro studies have also detected NAA expression in mature, immature, and undifferentiated oligodendrocytes.[29 30] Nevertheless, according to a recent study, in vivo MRS measurements of NAA remain axon specific, with no oligodendrocytes, nonproliferating oligodendrocyte progenitor cells, or myelin contributing to detectable NAA in the mature CNS.[31] This result supports the view that the widespread NAA/Cr reductions observed in this study ultimately reflect widespread neuronal and axonal involvement in MSA, although oligodendrocytes might influence the NAA levels to some degree.

The striking observation in this study is that the NAA/Cr reduction in the pontine base was the most significant among the three regions examined. That reduction was detected in the early phase of illness even in patients with no symptoms of ataxia or parkinsonism, or in patients without MRI abnormality of the HCB sign. Moreover, the pontine NAA/Cr reduction was significant even in MSA-P patients. In addition, NAA/Cr reductions in the pontine base were seen even in patients with no HPR sign in the lateral putamen. These observations suggest that NAA/Cr reduction in the pontine base is an accurate diagnostic marker for MSA even in patients in an early stage and a pre-symptomatic phase of ataxia or parkinsonism. The diagnostic focus of ^{1}H-MRS in MSA has been on the putamen,[11–14] whereas our results unequivocally demonstrated that MRS abnormality can be detected sooner and more universally in the pontine base than in the putamen in the course of the disease. The question is why a significant NAA/Cr reduction can be detected more readily in the pontine base than in the putamen. One reason may be that neuroaxonal degeneration

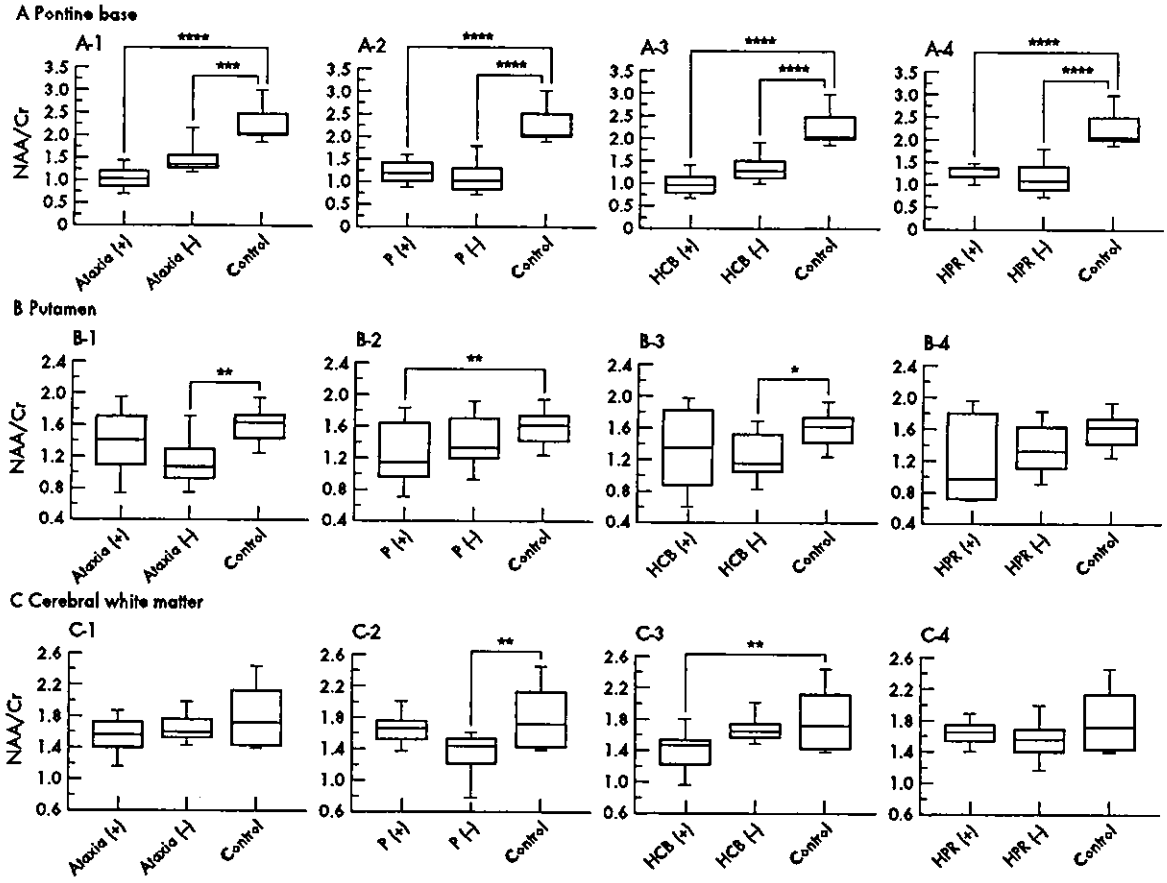

Figure 5 NAA/Cr in the pontine base (A), putamen (B), and cerebral white matter (C) for MSA patients classified in terms of clinical features of ataxia (+ or −; A-1, B-1, C-1), parkinsonism (P; + or −; A-2, B-2, C-2), HCB on MRI (+ or −; A-3, B-3, C-3), and hyperintense putaminal rim (HPR) on MRI (+ or −; A-4, B-4, C-4). +, Presence; −, absence. *p = 0.047, **p = 0.02, ***p = 0.0006, and ****p<0.0001 by Scheffé's test, respectively. NAA, *N*-acetylaspartate; Cr, creatine; MSA, multiple system atrophy; CWM, cerebral white matter.

in the pons would be more extensive than in the putamen. As the pontine base consists of the axons and neurones specifically involved in MSA (for example fibres of cerebellar inflow and outflow, corticospinal tracts and transverse pontine tracts), subclinical involvement of such fibres could be detected as a reduction of NAA/Cr. Furthermore, because, as we demonstrated previously, MSA-C is significantly more prevalent in Japan than MSA-P, compared with white populations in the western countries,[7] the cerebellar pontine system should be more profoundly involved in Japanese MSA patients. A second possibility is that the volume effect due to putaminal atrophy would ultimately include the neighbouring normal tissues in the VOI of the MRS, influencing the degree of the NAA/Cr reduction. As atrophy of the putamen is severe in certain patients, the size of the VOI is a limiting factor in ^{1}H-MRS for maintaining an acceptable SNR. Such volume effects due to putaminal atrophy can result in conflicting data. Clarke and Lowry reported an absence of significant reductions in basal ganglionic NAA/Cr in MSA,[16] precluding the use of NAA/Cr reductions in the striatum for differential diagnosis.[18] Disease duration in their patients averaged 7.9 years.[16] In contrast, mean disease duration in other reports showing significant NAA/Cr reductions in the striatum of MSA patients ranged from 3.2 to 4.5 years,[11–14] similar to the duration in our patients. Because, with longer duration, putaminal atrophy in patients with MSA-P becomes more severe, discrepancies could be explained by differences in putaminal atrophy that can profoundly influence ^{1}H-MRS results. By avoiding this volume effect, MRS for the pontine base would provide a more accurate diagnostic marker.

Discriminating clearly between MSA-P and PD has long been a diagnostic problem from both therapeutic and prognostic viewpoints. Putaminal NAA/Cr reduction was significant in MSA-P patients compared with PD and control subjects, as previously reported.[11–14] However, as discussed above, the putaminal volume effect could influence the significance of putaminal NAA/Cr reduction, particularly in patients with advanced disease. Although brainstem and cerebellar involvement is an important and specific finding in differentiating MSA-P from PD,[26 32] the sensitivity of both clinical and MRI evaluations of these abnormalities is relatively low.[7 26] Based on our results, we believe that ^{1}H-MRS assessment of the pontine base would be of considerable value in the differential diagnosis between MSA-P and PD. However, combined ^{1}H-MRS study of the pontine base and putamen can provide a more sensitive differentiation between MSA-P and PD than a conventional single regional study, such as that of the putamen.

The cerebral hemisphere is involved more extensively in MSA than previously believed. Recently, Abe *et al* reported a significant decrease in NAA/Cr in MSA, involving Brodmann's areas 6, 8, and 46.[14] Moreover, Spargo *et al*

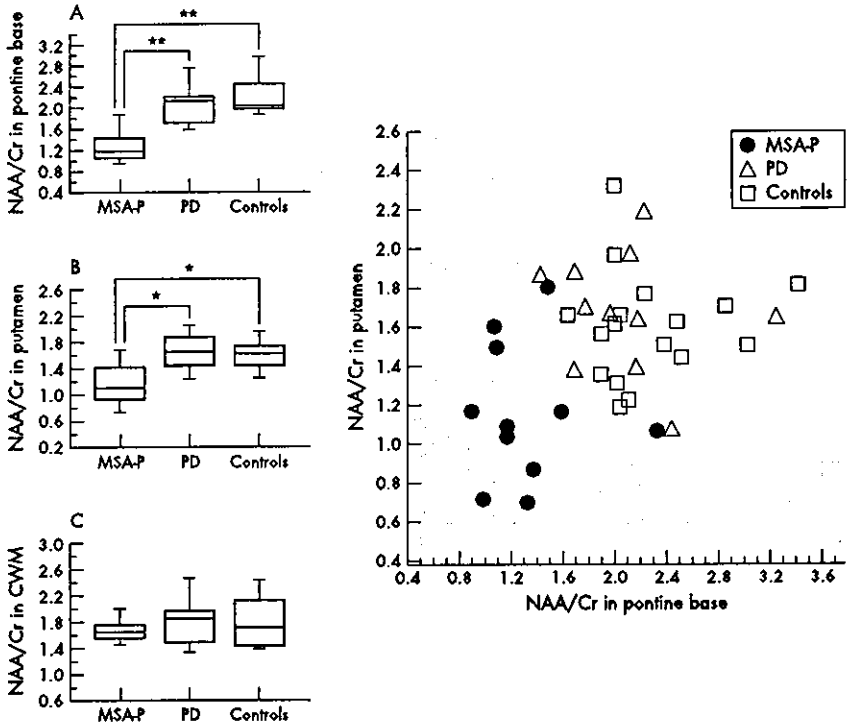

Figure 6 Box and whisker plot of the NAA/Cr ratio in the pontine base (A), putamen (B) and cerebral white matter (CWM, C) compared between MSA-P, PD, and controls. D is a scatter plot of the individual NAA/Cr data in the pontine base v putamen including MSA-P, PD, and control subjects. The scaled area corresponds to the mean−2 SD of NAA/Cr in the pontine base and putamen of control subjects. *p=0.002, **p<0.0001 by Scheffé's test, respectively. NAA, *N*-acetylaspartate; Cr, creatine; MSA-P, multiple system atrophy with parkinsonism predominant.

reported 18.7% and 21.4% neuronal loss in the primary and supplementary motor cortex, respectively.[33] In addition, the degree of atrophy in cerebral hemispheric areas varies between individuals, often becoming severe in long standing cases.[34] We found a mild overall reduction of NAA/Cr in CWM with a more significant NAA/Cr reduction in the subgroup with a longer duration of illness. This finding is in good agreement with previous ^{1}H-MRS reports and pathological observations.

Davie *et al*[11] reported a significant reduction of Cho/Cr ratio suggesting reduced membrane turnover in the lentiform nucleus in MSA, perhaps as result of cell loss. In the present study, Cho/Cr showed little change throughout the course of disease in the putamen, pontine base, and CWM, in agreement with other reports.[12–14 16] The relevance of this discrepancy is uncertain. One possible explanation is the difference of technical factors such as size of VOI and echo time. On the other hand, pathological study shows not only cell loss but also widely and variously distributed myelin degeneration in MSA brains that may increase the Cho.[33] Thus, heterogeneity of lesions in association with disease stage also may influence the Cho/Cr result. Further longitudinal studies and comparison of ^{1}H-MRS with histological findings will be needed to clarify the uncertainty as to the Cho/Cr ratio in MSA.

In conclusion, localised ^{1}H-MRS at 3.0 T in multiple regions showed widespread neuronal and axonal involvement in patients with MSA. NAA/Cr reduction in the pontine base provided a significant diagnostic marker for MSA irrespective of the disease form of MSA-P or MSA-C, disease duration, symptomatic manifestations, or MRI abnormalities. Moreover, combined ^{1}H-MRS study of the pontine base and putamen proved particularly effective in differentiating MSA from PD. We believe that ^{1}H-MRS would provide an early and accurate MSA diagnosis, an enhanced understanding of its pathogenetic mechanism, and the conclusiveness needed for future therapeutic trials.

Authors' affiliations

H Watanabe, M Katsuno, M Sugiura, K Hamada, Y Okada, M Hirayama, G Sobue, Department of Neurology, Nagoya University Graduate School of Medicine, Japan
H Fukatsu, T Ishigaki, Department of Radiology, Nagoya University Graduate School of Medicine, Japan

Competing interest: none declared

REFERENCES

1 **Graham JG,** Oppenheimer DR. Orthostatic hypotension and nicotine sensitivity in a case of multiple system atrophy. *J Neurol Neurosurg Psychiatry* 1969;**32**:28–34.
2 **Quinn N.** Multiple system atrophy–the nature of the beast. *J Neurol Neurosurg Psychiatry* 1989;**52**:78–89.
3 **Gilman S,** Low PA, Quinn N, *et al.* Consensus statement on the diagnosis of multiple system atrophy. *J Neurol Sci* 1999;**163**:94–8.
4 **Sobue G,** Terao S, Kachi T, *et al.* Somatic motor efferents in multiple system atrophy with autonomic failure: a clinico-pathological study. *J Neurol Sci* 1992;**112**:113–25.
5 **Wenning GK,** Ben-Shlomo Y, Magalhes M, *et al.* Clinicopathological study of 35 cases of multiple system atrophy. *J Neurol Neurosurg Psychiatry* 1995;**58**:160–6.
6 **Lantos P.** The definition of multiple system atrophy: A review of recent developments. *J Neuropathol Exp Neurol* 1998;**57**:1099–111.
7 **Watanabe H,** Saito Y, Terao S, *et al.* Progression and prognosis in multiple system atrophy; an analysis of 230 Japanese patients. *Brain* 2002;**125**:1070–83.
8 **Ross B,** Michaelis T. Clinical applications of magnetic resonance spectroscopy. *Magn Reson Q* 1994;**10**:191–247.
9 **Davie CA.** The role of spectroscopy in parkinsonism. *Mov Disord* 1998;**13**:2–4.
10 **Rudkin TM,** Arnold DL. Proton magnetic spectroscopy for the diagnosis and management of cerebral disorders. *Arch Neurol* 1999;**56**:919–26.
11 **Davie CA,** Wenning GK, Barker GJ, *et al.* Differentiation of multiple system atrophy from idiopathic Parkinson's disease using proton magnetic resonance spectroscopy. *Ann Neurol* 1995;**37**:204–10.
12 **Federico F,** Simone IL, Lucivero V, *et al.* Proton magnetic resonance spectroscopy in Parkinson's disease and atypical parkinsonian disorders. *Mov Disord* 1997;**12**:903–9.
13 **Federico F,** Simone IL, Lucivero V, *et al.* Usefulness of proton magnetic resonance spectroscopy in differentiating parkinsonian syndromes. *Ital J Neurol Sci* 1999;**20**:223–9.
14 **Abe K,** Terakawa H, Takanashi M, *et al.* Proton magnetic resonance spectroscopy of patients with parkinsonism. *Brain Res Bull* 2000;**52**:589–95.

15 **Terakawa H**, Abe K, Watanabe Y, *et al.* Proton magnetic resonance spectroscopy (1H MRS) in patients with sporadic cerebellar degeneration. *J Neuroimaging* 1999;**9**:72–7.
16 **Clarke CE**, Lowry M. Basal ganglia metabolite concentrations in idiopathic Parkinson's disease and multiple system atrophy measured by proton magnetic resonance spectroscopy. *Eur J Neurol* 2000;**7**:661–5.
17 **Hu MTM**, Simmons A, Glover A, *et al.* Proton magnetic resonance spectroscopy of the putamen in Parkinson's disease and multiple system atrophy. *Mov Disord* 1998;**13**:182.
18 **Clarke CE**, Lowry M. Systematic review of proton magnetic resonance spectroscopy of the striatum in parkinsonian syndromes. *Eur J Neurol* 2001;**8**:573–7.
19 **Bomsdorf H**, Helzel T, Kunz D, *et al.* Spectroscopy and imaging with a 4 Tesla whole-body MR system. *NMR Biomed* 1988;**1**:151–8.
20 **Hetherington HP**, Pan JW, Chu W-J, *et al.* Biological and clinical MRS at ultra-high field. *NMR Biomed* 1988;**10**:360–71.
21 **Gruetter R**, Weisdorf SA, Rajanayagan V, *et al.* Resolution improvements in vivo NMR spectra with increased magnetic field strength. *J Magn Reson* 1988;**135**:260–4.
22 **Calne DB**, Snow BJ, Lee C. Criteria for diagnosing Parkinson's disease. *Ann Neurol* 1992;**32**:S125–7.
23 **Savoiardo M**, Strada L, Girotti F, *et al.* Olivopontocerebellar atrophy: MR diagnosis and relationship to multiple system atrophy. *Radiology* 1990;**174**:693–6.
24 **Kraft E**, Schwarz J, Trenkwalder C, *et al.* The combination of hypointense and hyperintense signal changes on T2-weighted magnetic resonance imaging sequences: a specific marker of multiple system atrophy? *Arch Neurol* 1999;**56**:225–8.
25 **Konagaya M**, Sakai M, Matsuoka Y, *et al.* Pathological correlate of the slitlike changes on MRI at the putaminal margin in multiple system atrophy. *J Neurol* 1999;**246**:142–3.
26 **Schrag A**, Good CD, Miszkiel K, *et al.* Differentiation of atypical parkinsonian syndromes with routine MRI. *Neurology* 2000;**54**:697–02.
27 **Moffett JR**, Namboodiri MAA, Cangro CB, *et al.* Immunohistochemical localization of N-acethylaspartate in rat brain. *Neuroreport* 1991;**2**:131–4.
28 **Simmons ML**, Frondoza CG, Coyle JT. Immunohistochemical localization of N-acethylaspartate with monoclonal antibodies. *Neuroscience* 1991;**45**:37–45.
29 **Urenjak J**, Williams SR, Gadian DG, *et al.* Specific expression of N-acethylaspartate in neurons, oligodendrocyte type-2 astrocyte progenitors, and immature oligodendrocyte in vitro. *J Neurochem* 1992;**59**:55–61.
30 **Bhakoo KK**, Pearce D. In vivo expression of N-acetylaspartate by oligodendrocytes: implications for proton magnetic resonance spectroscopy signal in vivo. *J Neurochem* 2000;**74**:254–62.
31 **Bjartmar C**, Battistuta J, Terada N, *et al.* N-acetylaspartate is an axon-specific marker of mature white matter in vivo: a biochemical and immunohistochemical study on the rat optic nerve. *Ann Neurol* 2002;**51**:51–8.
32 **Litvan I**, Goetz CG, Jankovic J, *et al.* What is accuracy of the clinical diagnosis of multiple system atrophy? *Arch Neurol* 1997;**54**:937–44.
33 **Sparga E**, Papp MI, Lantos PL. Decrease in neuronal density in the cerebral cortex in multiple system atrophy. *Eur J Neurol* 1996;**13**:450–6.
34 **Konagaya M**, Sakai M, Matsuoka Y, *et al.* Multiple system atrophy with remarkable frontal lobe atrophy. *Acta Neuropathol (Berl)* 1999;**97**:423–8.
35 **Matsua A**, Akiguchi I, Lee GC, *et al.* Myelin degeneration in multiple system atrophy detected by unique antibodies. *Am J Pathol* 1998;**153**:671–6.

Sweet relief for Huntington disease

Masahisa Katsuno, Hiroaki Adachi & Gen Sobue

Oral delivery of a simple, nontoxic sugar molecule alleviates symptoms of Huntington disease in a mouse model (pages 148–154).

A CAG repeat was first pinned to a neurological disorder—spinal and bulbar muscular atrophy (SBMA)—in 1991 (ref. 1). The pathological influence of the affected gene, an androgen receptor, eventually paled beside the growing realization that the repeat itself was key to the disease. A number of other neurological diseases have since been linked to glutamine-encoding CAG repeats, most prominent among them Huntington disease.

Despite the excitement they have sparked, these discoveries have as yet done little to improve the lives of patients, including more than 35,000 with Huntington disease in the United States. In this issue, Tanaka *et al.* move us closer to reaping the benefits of this decade of research. The authors report that in mouse models of Huntington disease, treatment with a nontoxic sugar substance can prevent the development of the brain pathology associated with Huntington disease, and can delay the progress of symptoms such as motor dysfunction. The approach stands out as the most exciting therapeutic prospect to date for Huntington disease, and also holds promise for the entire class of polyglutamine disorders.

In addition to Huntington disease and SBMA, other polyglutamine disorders include several forms of spinocerebellar ataxia, as well as dentatorubral pallidoluysian atrophy[2]. Outside of the polyglutamine stretch, each causative protein seems unrelated, and removal of the causative protein genetically or by other means does not result in disease in humans or animal models[2]. Yet the diseases show phenotypic similarities. The clinical features depend at least partially on the number of CAG repeats, and are influenced by the meiotic instability of the repeat length. These clinical and genetic similarities imply that polyglutamines induce toxicity, although loss of the normal function of causative proteins may influence the disease[3].

Masahisa Katsuno, Hiroaki Adachi and Gen Sobue are in the Department of Neurology, Nagoya University Graduate School of Medicine, Nagoya, 65 Tsurumai-cho, Showa-ku, Nagoya 466-8550, Japan.
e-mail: sobueg@med.nagoya-u.ac.jp

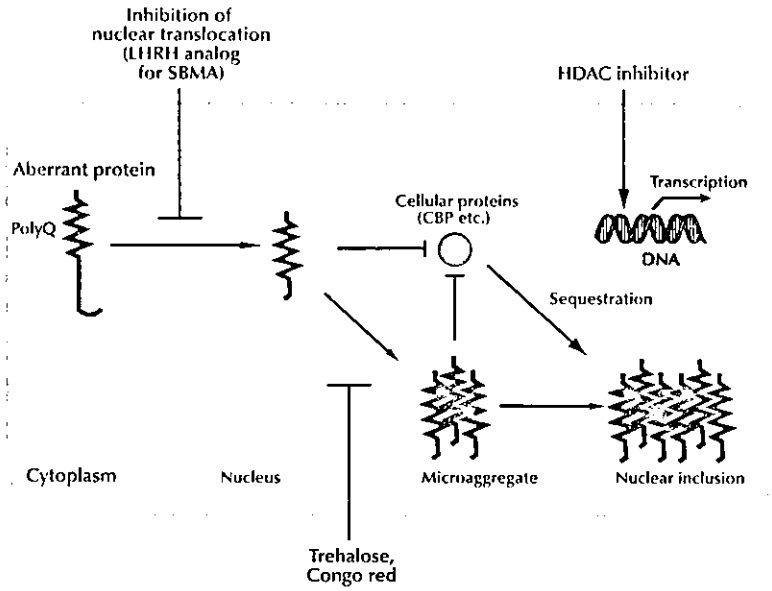

Figure 1 Therapeutic approaches for polyglutamine diseases. Several approaches attempt to mitigate the toxicity of polyglutamine (poly Q) tract–containing proteins. Leuprorelin prevents nuclear uptake of mutant androgen receptor, resulting in the rescue of neuromuscular phenotypes of SBMA. Histone deacetylase inhibitors ameliorate transcription of affected cells. Tanaka *et al.* found that a disaccharide, trehalose, inhibits aggregation of a protein with an expanded polyglutamine tract, especially in the nucleus (as does Congo red). LHRH, luteinizing hormone–releasing hormone; CBP, CREB-binding protein.

How do the glutamine repeats affect the cell? The expansion of the polyglutamine tract alters protein conformation, resulting in the formation of insoluble aggregates. These aggregates sequester normal cellular proteins such as transcription factors, heat shock proteins, ubiquitin, and proteasome components. The propensity of the polyglutamine-containing proteins to aggregate depends on the length of the polyglutamine stretch and is enhanced by protein cleavage through caspase activation.

Patients with polyglutamine diseases show loss of specific types of neurons. The cells that do not die contain inclusions rich in polyglutamine-containing proteins, mainly in the nucleus. These inclusions are found in the vulnerable neurons, implying a direct role in pathogenesis. Whether these aggregates are toxic—a notion supported by a large body of evidence—or reflect a protective response is controversial.

A dramatic study earlier this year bolstered arguments in favor of toxicity. Injection of the dye Congo red prevented formation of nuclear inclusions and alleviated symptoms in a mouse model of Huntington disease[4].

Tanaka *et al.*, favoring the notion that the aggregates are toxic, sought a new aggregation inhibitory therapy for Huntington disease[5]. The authors first used an *in vitro* aggregate formation assay, with myoglobin containing an expanded polyglutamine tract as a target molecule. Using this screening system, they discovered that disaccharides potently inhibited aggregate formation. Trehalose, the most effective disaccharide, selectively stabilized a protein containing a long polyglutamine tract, but not a protein with the normal number of glutamines. The authors confirmed this stabi-

lization in a cell model expressing the aberrant form of huntingtin, the causative protein of Huntington disease. The stabilization of myoglobin with an elongated polyglutamine tract results[6] accounts for the trehalose-mediated suppression of aggregation formation.

The authors went on to test transgenic mouse models of Huntington disease. They found that trehalose-treated mice had fewer nuclear inclusions than untreated mice. Trehalose also improved motor dysfunction and prolonged survival, without any deleterious side effects. The extremely low toxicity and high water-solubility of this compound make this an attractive therapeutic approach, although the therapeutic effects seem to result from prevention of new aggregate formation, not from reversal of the pathology. The data reinforce the rationale of aggregation-inhibitory therapy for polyglutamine diseases (Fig. 1). Trehalose is now ready for phase 1 safety trials in humans.

Other approaches to polyglutamine disease also show promise. Nuclear accumulation of polyglutamine-containing proteins before aggregate formation is probably an essential step in pathogenesis. A mutation that inactivates the nuclear localization signal in ataxin-1, the causative protein in spinocerebellar ataxia-1, nullifies polyglutamine-induced neurodegeneration in a transgenic mouse model[7]. In cell culture, chemically synthesized polyglutamine peptides induce neuronal cell death only when they are directed into the nucleus[8]. These observations suggest that nuclear-directed transport of mutant proteins is an alternative target of intervention (Fig. 1), although cytosolic events should not be neglected[3].

Androgen deprivation therapy in a transgenic mouse model of SBMA clearly demonstrates the usefulness of this therapeutic strategy[9]. A luteinizing hormone–releasing hormone analog, leuprorelin, prevents nuclear translocation of polyglutamine-containing androgen receptor protein, resulting in a significant improvement of disease[9]. A clinical trial with leuprorelin, currently under way in Japan, should clarify the clinical benefit of this drug for SBMA patients.

Transcriptional dysregulation, an event downstream of polyglutamine aggregation, can also be targeted (Fig. 1). Transcriptional coactivators including CREB-binding protein are sequestrated in the inclusion, and are also enfeebled by interaction with soluble polyglutamine tract–containing proteins[3]. An increase in acetylation of nuclear histone proteins, facilitated by histone deacetylase inhibitors, ameliorates neurodegeneration in a mouse model of Huntington disease[10,11]. These compounds have also been used for patients with malignancies. Clinical trials of histone deacetylase inhibitors should be planned carefully, however, taking the hazardous side effects into account.

The promising results of these preclinical studies are ushering in a new era in polyglutamine research: the therapeutic stage. The new investigations also encourage us to continue to search for new, clinically applicable compounds such as aggregation inhibitors. The intensive basic research is bearing fruit, and shows promise of continuing to do so as we move into clinical trials.

1. La Spada, A.R. *et al. Nature* **352**, 77–79 (1991).
2. Zoghbi, H.Y. & Orr, H.T. *Annu. Rev. Neurosci.* **23**, 217–247 (2000).
3. Ross, C.A. *Neuron* **35**, 819–822 (2002).
4. Sanchez, I. *et al. Nature* **421**, 373–379 (2003).
5. Tanaka, M. *et al. Nat. Med.* **10**, 148–154 (2004).
6. Tanaka, M. *et al. J. Biol. Chem.* **276**, 45470–45475 (2001)
7. Klement, I.A. *et al. Cell* **95**, 41–53 (1998).
8. Yang, W. *et al. Hum. Mol. Genet.* **11**, 2905–2911 (2003).
9. Katsuno, M. *et al. Nat. Med.* **9**, 768–773 (2003).
10. Hockly, E. *et al. Proc. Natl. Acad. Sci. USA* **100**, 2041–2046 (2003).
11. Ferrante, R.J. *et al. J. Neurosci.* **23**, 9418–9427 (2003).